www.nature.com/scientificreports

scientific reports

OPEN

Egyptian basalt powder as a fortifier for improved performance and sustainability of alkali-activated slag cement

Alaa M. Rashad[1]✉, M. H. El-Nashar[2], Omnia Farouk Hussien[3] &
Reham Abu-Elwafa Mohamed[4]

As is well established, slag precursor offers promising performance characteristics; however, its origin as an industrial byproduct leads to variability in both mineralogical and chemical composition. Furthermore, the global availability of slag is limited compared to that of Portland cement (PC), raising concerns about long-term supply stability. To address these issues, this study investigates the incorporation of natural materials—specifically Egyptian natural basalt powder (BP)—as a partial replacement for slag. The research explores BP as a supplementary component in alkali-activated slag (AAS) systems. Blends containing 2.5 wt% to 40 wt% BP were prepared, and both pure slag and slag/BP mixtures were subjected to alkali activation to produce BP-modified AAS cement. The study aimed to assess the impact of varying BP ratios on flow characteristics, setting time, compressive strength, resistance to simulated real-world environmental conditions, and transport properties of the produced cement cured in air and water. In addition, the impact of varying BP ratios on drying shrinkage was monitored. This study also involved interpreting the key results through the use of a variety of contemporary scientific tools. Notwithstanding, BP might have slightly hindered the mixture flowability (up to 10.9% reduction) and prolonged setting time (1.23-fold for initial and 1.28-fold for final setting), the results demonstrated that including 2.5–20% BP improved the overall properties of the cement. An optimal ratio of 20% yielded the highest compressive strength, with an increase of up to 17.65% at 90 days under water curing, the lowest transport properties, with a decrease of 20%, and the lowest strength loss (3.63%) due to environmental conditions exposure under water curing, alongside reduced drying shrinkage. However, including 30% BP showed only a marginal effect, whilst including 40% BP showed a detrimental effect. Additionally, water curing proved superior to air curing, exhibiting higher strength, lower transport properties, and mitigating microcrack formation, thereby enhancing durability against wetting-drying cycles.

Keywords Alkali-activated slag, Basalt powder, Fresh properties, Transport properties, Environmental conditions, Compressive strength

The Portland cement (PC) industry is a major driver of climate change, of which producing one tonne of cement generates 810 kg CO_2, a major greenhouse gas, as well as 2 kg NOx, a contributor to smog, and 1 kg SO_2, a source to acid rain. Currently, this industry accounts for roughly 7% of the overall emissions[1]. Without any alteration, by 2025, this proportion could exceed 25%[2]. Although CO_2 effectively transmits sunlight, it traps infrared radiation, preventing its escape from Earth. This occurrence is called the “Greenhouse Effect”, which is crucial for maintaining Earth’s warmth, but also contributes to global warming due to increased heat-trapping[3]. This changing climate poses a serious threat to human health, with consequences for the cardiovascular and respiratory systems. This could manifest as declining lung function, compromised cardiovascular health, increased incidence of chronic obstructive pulmonary disease-related hospitalization and mortality, and heart disease[4]. Melting ice caps, increasing sea levels, and escalating temperatures are just some of the harmful

[1]Building Materials Research and Quality Control Institute, Housing and Building National Research Center (HBRC), Cairo, Egypt. [2]Building Physics and Environmental Research Institute, Housing & Building National Research Center (HBRC), Cairo, Egypt. [3]Faculty of Engineering, Egyptian Russian University, Cairo, Egypt. [4]Raw Building Materials Technology and Processing Research Institute, Housing and Building National Research Center (HBRC), Cairo, Egypt. ✉email: alaarashad@yahoo.com

influences of surplus CO_2 emissions on the environment, highlighting the urgent need for action to address this occurrence[5]. This industry relies heavily on energy; roughly 4 to 5 GJ/tonne of energy is consumed[6]. It relies heavily on virgin materials, which can lead to resource depletion. Additionally, this industry is criticized for contributing to elevated noise pollution from the extraction phase to the delivery of the final product[7]. Several measures have been put in place to alleviate these issues, aiming for a reduction of 80–90% by the year 2050, with 1990 as the reference point[8]. One way to meet these goals is by mixing cement with fly ash (FA)[9], pumice[10], metakaolin (MK)[11,12], slag[13], and others. Another effective way is to employ alkali-activated materials (AAMs).

Because of their clear advantages in terms of performance, economy, and the environment over PC, AAMs present an auspicious substitute. The alkali activation mechanism is a multifaceted polycondensation process initiated by a highly alkaline solution. It generally proceeds through three stages: (1) Dissolution, where the glassy matrix of precursors such as slag is depolymerized under high pH, breaking Si–O–Si, Si–O–Al, and Al–O–Al bonds and releasing silicate and aluminate species, along with cations like Ca^{2+}; (2) Reorganization and polycondensation of these species into a reactive sol-gel; and (3) Hardening, during which the gel network evolves into an amorphous or semi-crystalline three-dimensional structure. In calcium-rich systems like alkali-activated slag, the dominant binding phase formed is C–S–H gel[14]. The incorporation of a silica-rich material such as basalt powder promotes the formation of a secondary, low-calcium N-A-S-H geopolymer gel[15]. This results in the coexistence of multiple gel phases, potentially enhancing the synergistic interactions within the binder matrix[16–19]. AAMs harness a range of industrial by-products like FA[20], mining leftovers[21], and slag[22,23], contrary to PC, which is primarily dependent on the calcination of limestone. By repurposing these materials into valuable construction products, AAMs not only reduce carbon emissions but also alleviate waste disposal concerns[24,25]. Moreover, AAMs boast exceptional durability, exceeding PC performance[26]. Adopting concrete made of AAMs has the potential to limit industrial waste by about 12.2 Mt annually[27]. FA[20], slag[22], and MK[28] are the most prevalent materials for precursors. Of these precursors, slag stands out as the most preferred due to its advantageous calcium ratio, which contributes to efficient curing conditions, as well as its optimal alumina to silica ratio. Specifically, ground granulated blast furnace slag (GGBFS) was deliberately selected for this study over other slag types, such as electric arc furnace (EAF) slag, due to its high amorphous phase content, superior reactivity, and consistent chemical profile. These characteristics ensure a stable and reliable foundation for investigating the impact of basalt powder. By contrast, the chemical variability and the presence of free lime and magnesia in EAF slag pose a risk of volumetric instability, potentially compromising result consistency[29–31]. Since the identification of slag-based binder materials in 1908, their development has rapidly advanced[32]. Kuhl initiated studies in 1930 on the activation of slag powder with caustic potash, marking the introduction of alkali cement. In 1937, Chassevent explored the reactivity of slag powder with soda and potash, further expanding knowledge in this area. By 1940, laboratory research on clinker-free cement made from slag activated by caustic alkalis or soda established a foundation for utilizing alkaline salts and bases in cement production. Then, in 1957, Glukhovsky introduced a new class of binders derived from calcium-free or low-basic calcium aluminosilicates activated with alkali metals. Since that time, alkali-activated materials, commonly referred to as geopolymers, have gained widespread attention as the construction industry increasingly seeks innovative materials with lower environmental impact. This binder has evolved and improved swiftly, continuously adapting to meet modern engineering demands and sustainability goals[33]. Scholars have explored a variety of techniques to enhance the activated slag efficiency. One such method involves slag grinding to a finer texture, which improves its capacity to establish robust binders. Alternative techniques include fibers[34–36], or even micrometer-sized particles[37], or nanometer-sized particles[38] into the composition. The utilization of mineral admixtures continues to be widely adopted, as they provide several options that are readily accessible. They can be arranged into foremost groups: natural materials like $Ca(OH)_2$[39], pumice[10], MK[40], $CaCO_3$[41], feldspar[42], CaO[43], volcanic glass[44], etc.; and byproducts like silica fume (SF)[33], waste of marble[45], and ceramic[46].

While slag exhibits promising properties as a precursor, its original use as a byproduct of the CO_2-producing industry results in inconstant mineralogical and chemical compositions. This issue poses a challenge in standardizing an alkali activation method for its market entry. The annual global production of slag (400–500 Mt) is limited compared to PC (4.1 billion Mt)[47]. Furthermore, the global demand for slag by 2030 is significantly smaller than that of PC[48]. Blending slag with natural materials can improve the properties of the resulting composite, offering a solution to these concerns. Regarding this situation, Rashad et al.[44] and Wang et al.[49] recognized improved compressive strength of AAS pastes by introducing 10% volcanic glass. The use of up to 70% volcanic glass as a partial substitution for slag in AAS mortars can mitigate alkali-silica reaction expansion[49]. Substituting slag with 70% volcanic ash enhanced the AAS binders' compressive strength, making them more operative for soil stabilization[50]. The incorporation of 10% feldspar into concrete made from AAS increased splitting strength, abrasion resistance, and compressive strength[42]. It was proposed that including 15% limestone powder in AAS matrices increased abrasion resistance, aging resistance, and compressive strength[51] but decreased drying shrinkage[52]. Substituting slag with natural pozzolan led to 25% improvement in 90-day compressive strength[53]. The use of up to 30% natural quartz powder as a partial substitution of slag in AAS pastes increased the resistance to thermal cycles[54] and compressive strength[55]. Substituting slag with 10% calcined talc can decrease the porosity of AAS pastes[56].

Basalt is a ubiquitous rock, found in the Earth's crust. It occupies about 70% of the crust of the Earth. SiO_2 constitutes the primary component, succeeded by Al_2O_3, in addition to Fe_2O_3, CaO, FeO, and MgO. According to its silica ratio, basalt is categorized as mildly acidic, alkaline, and acidic when the silica ratio is 43–46%, up to 42%, and over 46%, respectively[57]. Its crystalline structure changes depending on the particular circumstances surrounding the flow of lava at each site. It typically appears in shades of gray to black, but it quickly alters to rust-red or brown, affected by oxidants. It has a long history of use in casting techniques, particularly for creating slabs and tiles. Beyond this, cast basalt liners for steel pipes demonstrate exceptional abrasion resistance, making them well-suited for demanding industrial settings[58]. It can be utilized as fibers[59–62], an aggregate[63], or a cementitious matrix for conventional PC[64,65]. Owing to its high level of silica and appropriate level of alumina, basalt powder can now be utilized as an AAM precursor or as a precursor component. It was verified that curing conditions have a weighty effect on the geopolymer paste made of BP[66]. Similarly, it was found that the NaOH molarities and curing conditions have a considerable effect on geopolymer pastes made of BP combined with glass powder[67]. It was reported that geopolymer pastes made of BP exhibited lower compressive strength than those made of 100% slag[68]. The results reported in[69] revealed that the flowability and mechanical strength of geopolymer pastes made of 50% BP/50% slag were affected by activator concentration/type. The compressive strength of AAS mortars and those with 20% waste BP sharply declined after exposure to high temperatures up to 900 ℃[70]. Including BP up to 20% into FA geopolymer pastes reduced transport properties but enhanced compressive strength[63]. This investigation builds upon the authors' previous work while exploring a fundamentally different material synergy. Our prior research successfully demonstrated the potential of Egyptian volcanic glass powder on AAS cement[44], establishing the viability of using natural pozzolans in this high-calcium system. Separately, we have also confirmed the effectiveness of BP for improving the properties of low-calcium, FA-based geopolymer cement[15]. The present study marks a critical and novel advancement by bridging these two areas of research: for the first time, we investigate the interaction between BP and a high-calcium alkali-activated slag system. This is a significant scientific distinction, as the reaction chemistry and performance mechanisms are entirely different. In the FA system, the binder is a N-A-S-H gel, whereas the slag system is dominated by the formation of C-S-H gel. Therefore, the unique contribution of this work is the first comprehensive evaluation of basalt powder's role as a fortifier specifically for AAS cement, elucidating its performance within a co-existing C-S-H/N-A-S-H hybrid binder matrix, a topic not addressed in our previous publications.

Despite the potential of basalt, studies on its use in AAS cement remain scarce. Most existing research focuses on geopolymer systems based solely on BP or in combination with FA, leaving a significant gap in understanding its synergistic effects as a partial substitute for slag. This study aims to fill this gap by conducting the first comprehensive investigation into the use of Egyptian BP as a fortifier in AAS cement, aiming to improve its performance and sustainability. The findings are expected to provide valuable insights into the development of more sustainable construction materials. Despite the limited studies in this area, Egypt boasts an abundance of basalt deposits across regions such as the west of the Red Sea Hills[71,72], the Eastern Desert[73], Cairo (near the Giza Pyramids)[74], and various volcanic terrains across the nation[75]. Ground basalt, when processed into fine basalt powder, exhibits remarkable pozzolanic properties, making it an innovative component for sustainable construction materials. Integrating BP into AAS cement presents significant environmental and economic benefits. Locally sourcing BP reduces reliance on imports, thereby cutting down costs and minimizing the carbon footprint associated with cement production. This approach aligns seamlessly with Egypt's national objectives for sustainable construction, resource efficiency, and industrial carbon emission reduction. Furthermore, leveraging BP fosters the development of durable, eco-friendly, and high-performance AAS cement-based materials. This not only enhances the technical attributes of alkali-activated cements but also contributes to global advancements in material innovation. Inspired by Egypt's commitment to sustainability and driven by the availability of BP and waste slag, this research delves into the potential of integrating BP into AAS cement. The aim is to unlock new opportunities for Egypt's construction sector while advancing global sustainable construction practices. To investigate this, slag was systematically substituted with BP at incremental levels ranging from 2.5 to 40%. Experimental specimens underwent two distinct curing methods: air curing and immersion in water at ambient temperature. A comprehensive evaluation was performed to measure key parameters including flow rate, setting time, environmental resistance, compressive strength, drying shrinkage, and transport properties. The experimental findings were meticulously analyzed using advanced scientific tools to ensure reliable conclusions.

Experimental details

Materials

The same supplier mentioned in[76] supplied the slag. The Egyptian natural basalt in powder form, used in this study, was supplied by a local cement factory. Both slag and BP have approximately the same specific gravity of 2.9. The average slag particle size was 37.183 µm (Fig. 1a), whilst it was 22.01 µm for BP (Fig. 1b). Table 1 demonstrates the chemical composition of each type of powder. Clearly, slag is a rich material of calcium, which has a positive influence on its curing. Evidently, whilst BP and slag share a similar alumina content, they differ in their silica and calcium. BP has higher silica content than slag, but a lower calcium content. Figure 2 demonstrates the XRD patterns of slag (Fig. 2a) and BP (Fig. 2b). The broad hump detected between 25° to 35° 2θ in Fig. 1a verified that the slag analyzed in this study is primarily amorphous[44]. The BP pattern reveals the crystalline phases of plagioclase (anorthite/albite), diopside, labradorite, and augite (Fig. 2a)[63,77]. Figure 3 demonstrates the overview of each type of powder. Figure 4 demonstrates the SEM images of each type of powder. The slag particles possess a jagged, irregular, and angular shape (Fig. 4a), whilst BP particles possess a granular texture with angular to subrounded shapes (Fig. 4b). NaOH and sodium silicate, obtained locally, meet the specifications in[44].

Mix proportion

The control mixture, coded 0B, comprised solely slag, with no BP added. The slag's weight was progressively replaced at six different ratios. These ratios were 2.5% (2.5B), 5% (5B), 10% (10B), 20% (20B), 30% (30B), and 40% (40B). A constant activator concentration (30%) was employed throughout the experiment to focus on the effect of varying BP ratios on AAS cement properties. The activator solution was comprised of 1: 2 parts of NaOH and sodium silicate[45]. A 10 M solution of NaOH was created, and this preparation proceeded at least one day before casting. To ensure consistent mixing conditions, supplementary water/powder(s) was established at a ratio of 10% for all mixtures. Mixture details are in Table 2. The mixing and casting processes adhered to the procedures mentioned in[17]. In short, slag and BP materials were pre-mixed for 4 min. The activator solution was

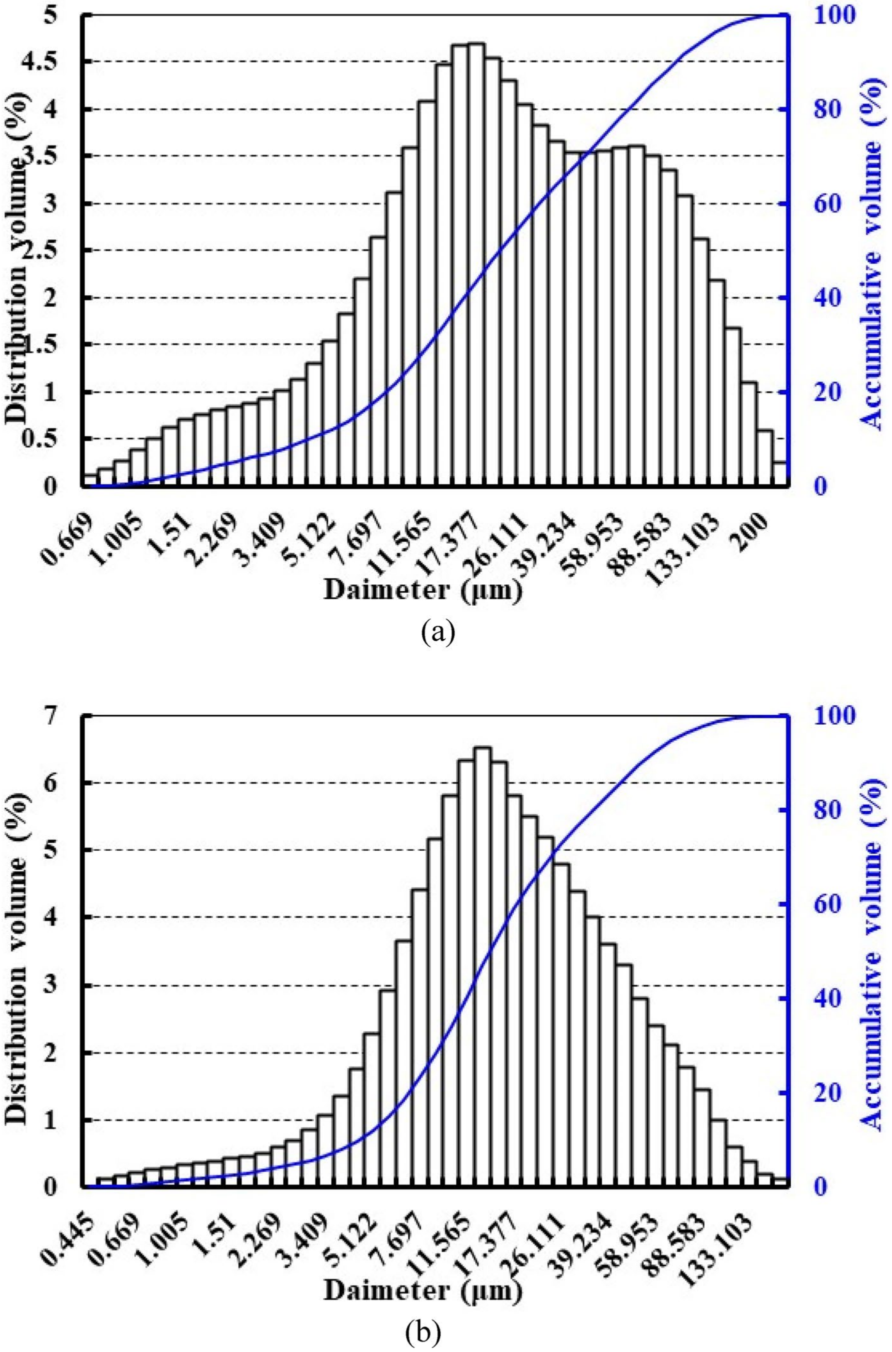

Fig. 1. Particle size distribution of slag (**a**), and BP (**b**).

Material	Oxide (%)												
	SiO_2	CaO	Fe_2O_3	Al_2O_3	MgO	SO_3	Na_2O	P_2O_5	Cl^-	K_2O	SrO	Other	L.O.I.
Slag (%)	31.45	39.44	1.45	15.64	6.08	1.83	1.81	0.03	0.16	0.91	0.14	0.56	0.5
BP (%)	50.38	7.2	14.3	15.41	4.31	0.12	2.54	0.57	0.02	1.2	0.09	2.84	1.02

Table 1. Chemical composition of slag and BP.

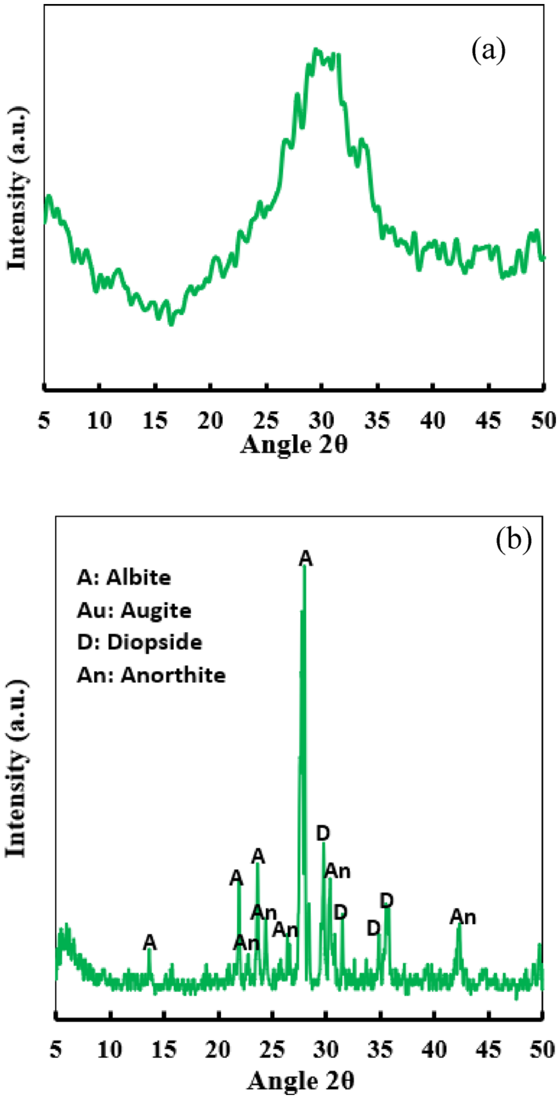

Fig. 2. XRD patterns of slag (**a**), and BP (**b**).

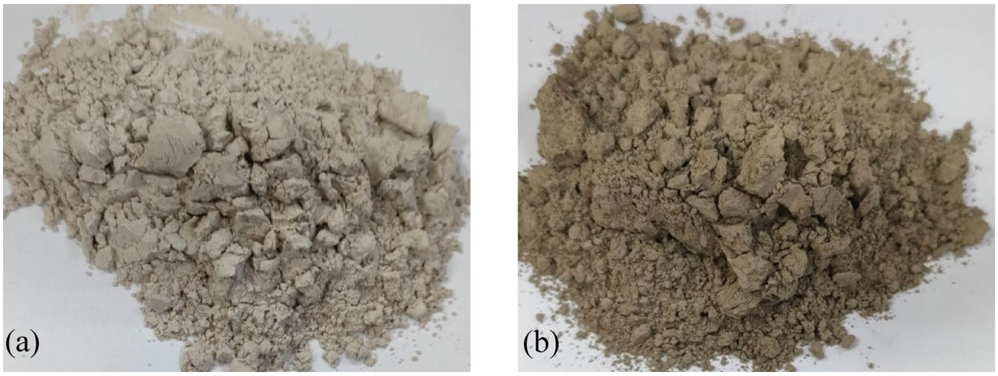

Fig. 3. Overview of slag (**a**), and BP (**b**).

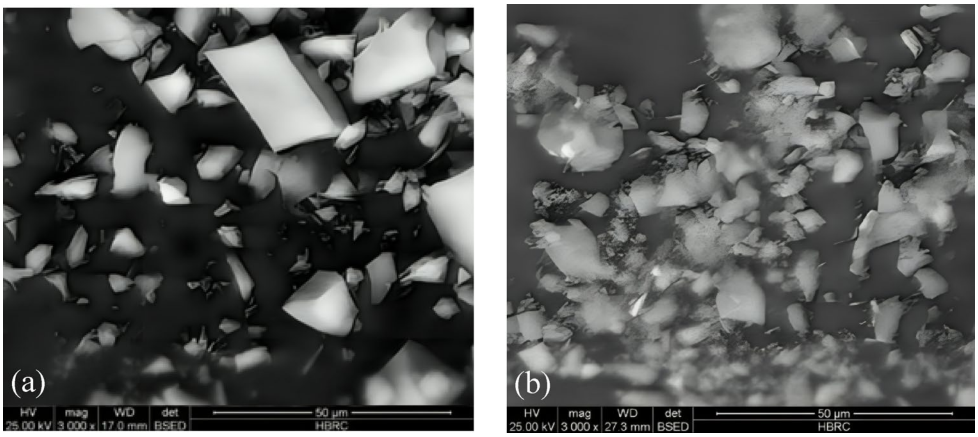

Fig. 4. SEM images of slag (**a**), and BP (**b**).

ID	Slag	BP	NaOH	Sodium silicate	Extra water
0B	400	0	40	80	40
2.5B	390	10			
5B	380	20			
10B	360	40			
20B	320	80			
30B	280	120			
40B	240	160			

Table 2. Mixture details (kg/m^3).

then incorporated and mixed with either slag alone or the slag-BP mixture for a duration of 5 min. The mixer was subsequently halted to collect and reintegrate any residual powder adhering to the bowl or paddle. After completing the 5 min mixing phase, the resulting mixture was cast into molds, and the molds were vibrated for 1 min to ensure air bubble removal.

Testing methods

Shortly after mixing, the fresh paste's physical behavior was evaluated. Flowability was determined with a flow table test in line with ASTM C230/C230M-23. Initial and final setting times were obtained using the Vicat apparatus, applying the standard procedure from ASTM C191-08. After demolding, half of the 25 mm cube specimens were air-cured, while the remaining half were immersed in water at room temperature. After curing, compressive strength assessments were performed on 25 mm cube samples at 7, 28, and 56 days of curing using a universal testing machine, in compliance with ASTM C109/C109M. The values reported reflect the mean of four measured specimens. To investigate the effect of environmental conditions on the performance of various specimens, after 28 days, the specimens were subjected to 40 wetting/drying cycles. Every cycle included soaking the specimens in water for a day at 20 ℃, then drying them in the air lab for another day. This approach was utilized to mimic the alternating conditions of rainy days and cloudy days[17,44,78,79]. To evaluate transport properties, hardened paste samples were tested at 28 days per ASTM C642-21, which involves weighing specimens in saturated, oven-dried, and suspended states. Drying shrinkage of 25 × 25 × 285 mm prism specimens, cured under controlled conditions of 23 ± 2 ℃ with 50 ± 4% RH[80], was measured immediately after demolding and throughout 56 56-day period using a length comparator with 0.001 mm accuracy, following ASTM C157/C157M standards and similar to[80–83]. Consistent with the approach reported in[46], the selected samples taken from the debris were tested by XRD, TGA/DTG, and SEM. Figure 5 demonstrates a visual representation of the experimental work.

Data presentation and analysis

This study was designed as an exploratory investigation to identify significant performance trends across a wide range of compositions. Therefore, the analysis focuses on the magnitude and consistency of the observed effects, which are presented as the mean and standard deviation of four replicates.

Results and discussions

Flowability

Figure 6 demonstrates how varying BP ratios influence the mixture flowability. According to preliminary findings, the 0B mixture, lacking BP, exhibits 94 ± 5% flow. This flow is considerably the highest among all tested mixtures. 0B's flowability seems to be within a tolerable range, exceeding those described in[17,84–87], but remaining

Fig. 5. A visual representation of the experimental work. *Note*: 1,2, weighting precursors, activator, and extra water; 3,4, mixing; 5, measuring flowability; 6, measuring setting time; 7,8, curing in air and water; 9, measuring compressive strength; 10, measuring drying shrinkage.

lower than those described in[44,68,88–91]. The measured flow of 0B falls within the range mentioned in past studies. Correspondingly, substituting a portion of slag with BP results in a slight decrease in flowability. This relationship is clear as the BP ratio rises, leading to less flowability. When the BP ratio was 2.5% (2.5 B), a marginal decrease in the flow was obtained (0.54%). However, when the ratio was 40% (40B), a somewhat obvious decrease in the flow was obtained (10.9%). The crushed particle's angular shape, coupled with the BP's higher fineness, contributes to the decreased flowability. This is a well-understood phenomenon in particle rheology; the finer BP particles possess a significantly higher specific surface area compared to slag, which increases the water demand required to wet the particle surfaces. This reduces the amount of 'free' water available to lubricate the paste, thereby increasing its viscosity and reducing flow[92]. Furthermore, the angular particle morphology increases inter-particle friction and mechanical interlocking, which further hinders the paste's ability to deform and flow under its own weight. It is important to indicate that introducing BP into conventional PC mixtures negatively influenced the workability[93].

Setting time

Figure 7 demonstrates how variable BP ratios affect the setting time. Preliminary findings suggest that the 0B mixture, devoid of BP, sets most rapidly among the tested mixtures. The 0B mixture has an initial setting of 88 min and a final setting of 188 min. Compared to the setting times documented in[17,91,94,95], these setting times are longer. However, they are shorter than those found in[44,87,96]. This implies that the measured setting times fall somewhere in the middle of those that have been previously measured. The setting time is directly influenced by the BP ratio. The overall results indicate that an increased BP ratio is associated with a longer setting time. The rate of prolonging seems to be marginal when 2.5–10% BP was used. However, the prolonging rate increases when 20–40% BP was used. For instance, the average increase in setting times with including 10% BP (10B) was 6.8%, whilst it was 26.3% with including 40% BP (40B). Calcium-rich slag chemical dilution is linked to the prolonged setting time when silica-rich BP was incorporated. The dilution causes a decrease in calcium amount, which is essential for the setting procedure[90]. The SiO_2/Al_2O_3 ratio increased with adding BP. Studies have shown that a higher SiO_2/Al_2O_3 ratio correlated with prolonged setting time[97]. However, the magnitude of this increase is moderated by a competing physical mechanism. The finer BP particles provide a high surface area, acting as numerous heterogeneous nucleation sites for the precipitating hydration products. This 'filler effect' facilitates the formation of a solid network structure, partially counteracting the chemical retardation. The observed setting time is therefore the net outcome of these two effects, explaining the moderate, rather than dramatic, prolongation even at high BP levels. It is important to mention that some studies have shown that replacing part of slag with alumina and silica-rich materials[98], or just silica[99], prolonged setting time. It is valuable to state that Venyite et al.[100] found a longer setting time of geopolymer pastes made of calcined laterites/MK/BP with an increase in BP amount. In conventional cement, Laibao et al.[101] found a longer setting time of cement pastes with increasing PB amount.

Compressive strength

Figure 8 demonstrates the progression of compressive strength for both plain AAS pastes and those comprising variable BP ratios treated in air. Both curing time and BP ratio exhibit a pattern in compressive strength, with longer curing times consistently leading to higher strength. The 0B specimens demonstrate satisfactory strength, reaching 77.81 MPa at 28 days. This result falls below those declared in[102,103], whilst surpassing those declared in[84,86,89]. Overall, the 0B compressive strength is consistent with earlier studies. Including 2.5% BP (2.5B) and 5% PB (5B) in the specimens exerts a slight beneficial influence on the compressive strength, revealing an average

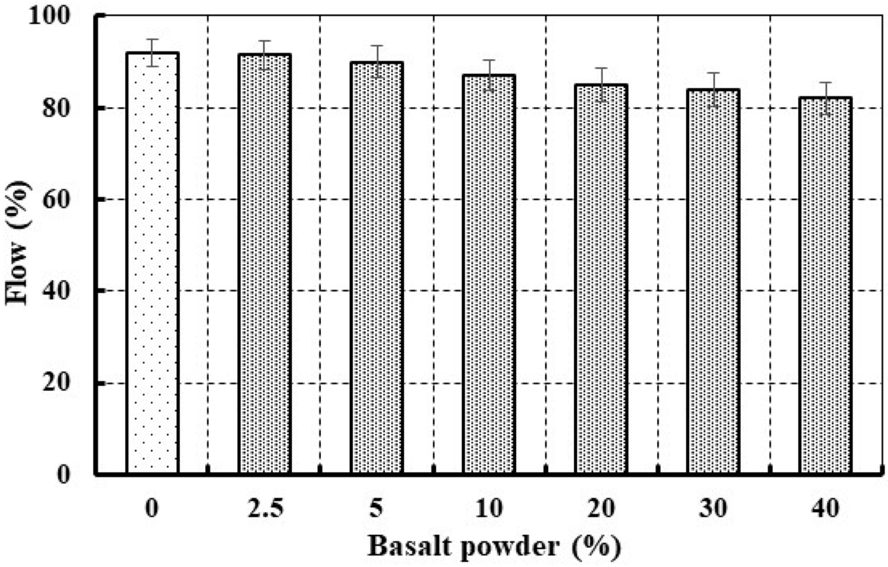

Fig. 6. Flowability changes with varying BP ratios.

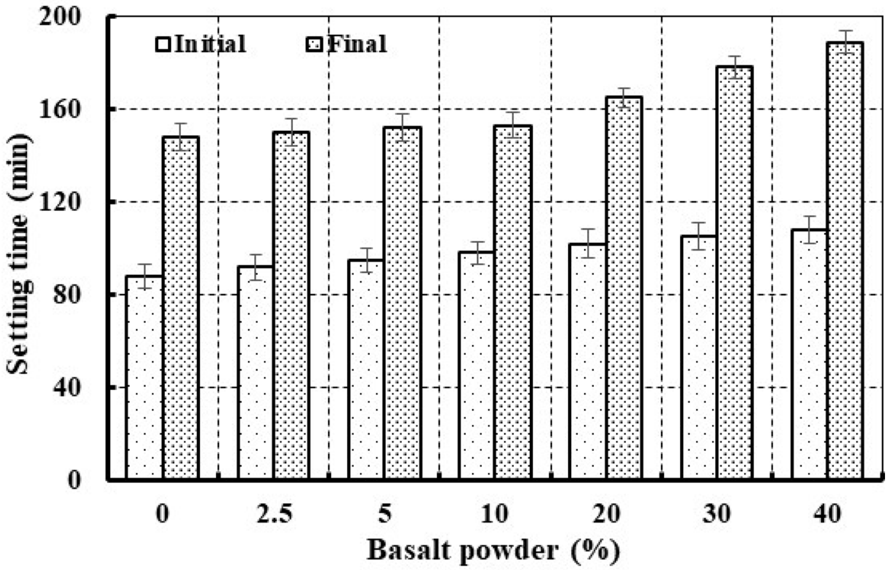

Fig. 7. Setting time changes with varying BP ratios.

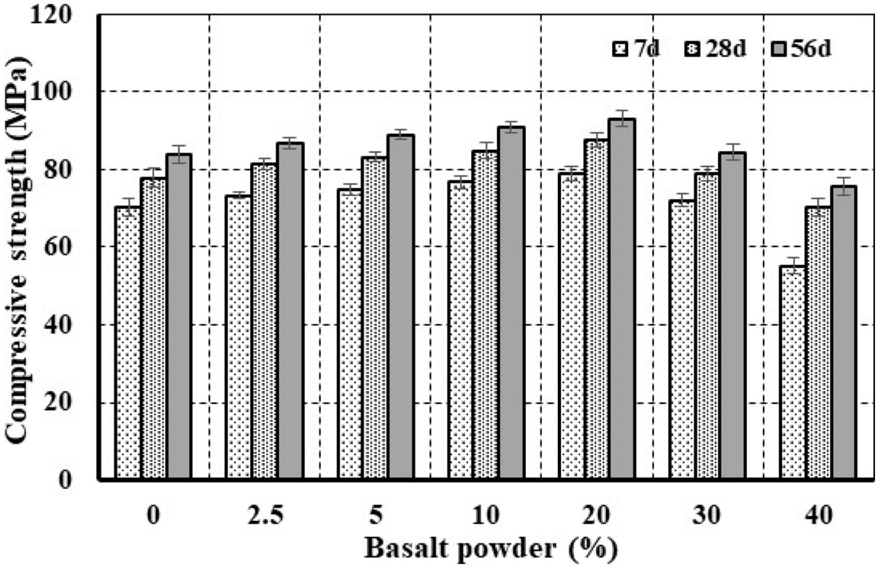

Fig. 8. Compressive strength changes with varying BP ratios for air cured specimens.

improvement of 4.26% and 6.6%, respectively. With 10% BP (10B) leads to an additional increase in strength, averaging ~ 9%. The maximum strength was obtained when 20% BP (20B) was included, averaging 12.1%. Including BP up to 20% not only improves AAS cement compressive strength but also enhances FA geopolymer cement compressive strength[63]. There are multiple reasons for improving strength with incorporating up to 20% BP. The BP fine particles, which can operate as microaggregates, is one likely contributing factor. The microaggregates can function as nucleation sites within slag particles. This process helps to refine microstructure and reduce porosity (see Sect. Microstructure analysis later), and ultimately enhances the strength[104]. Another reason is the increased SiO_2/Al_2O_3 ratio. This ratio rises from 4.05 for 0B to 4.47 for 20B. It is widely recognized that a higher SiO_2/Al_2O_3 ratio, up to a certain point, favors the polysialatesiloxo and polysialatedisiloxo structures formation over polysialate structures[105]. This suggests that keeping an optimum SiO_2/Al_2O_3 is necessary for creating strong geopolymeric materials. Ratios exceeding or falling short of this ideal ratio can lead to a less stable polymerized network, compromising the material's strength[106]. An additional contributing factor is the formation of N-A-S-H gel resulting from the inclusion of BP, which can coexist with the C-S-H gel produced by slag.

Contrarily, the incorporation of BP at levels higher than 20% adversely affects the strength. For instance, using 30% BP (30B) results in an average strength decrease of 9.37% compared to 20B, but still marginally higher than 0B. The most substantial decline in strength, at 22.54% compared to 20B and 13.18% compared to 0B, occurs when the highest amount of BP (40B) was used. This reduction is a direct consequence of the 'dilution effect,' a principle consistently observed when a highly reactive precursor like slag is replaced by a less-reactive, silica-rich material. This effect has been documented in alkali-activated slag systems blended with volcanic glass[44], feldspar[104], and even basalt powder itself[68]. At high replacement levels, the significant reduction in the primary binder (slag) leads to an insufficient volume of reactive calcium to form a continuous, dense C-S-H gel matrix. While the basalt powder contributes to a secondary N-A-S-H gel, its reaction kinetics are slower and its volumetric contribution is insufficient to fully compensate for the loss of the primary, fast-reacting, strength-giving phase from the slag, resulting in a more porous and weaker composite. Furthermore, using SiO_2/Al_2O_3 ratios higher than the ideal can hinder gel formation and stability. As a result, there are more nonreacted particles present, the microstructure becomes porous, and the strength eventually reduces[107]. Likewise, the strength of AAS mortars[108], concretes[104], and pastes[109] improves when slag was combined with a highly silica-rich material up to a particular ratio. However, if the silica ratio surpasses the ideal, the strength decreases.

Figure 9 demonstrates the progression of compressive strength for both neat AAS pastes and those comprising different BP ratios cured in water. The overall pattern of the findings presented in Fig. 9 is generally comparable to those displayed in Fig. 8, although with an increased level of compressive strength. The optimal BP ratio (i.e., 20%) shows a 17% increase in the average compressive strength (18.81% at 7 days, 14.54% at 28 days, and 17.65% at 90 days). The greater compressive strength observed in Fig. 9 compared to Fig. 8 may be associated with the decrease in cracking propensity achieved through water curing[110,111] (see Sect. Microstructure analysis later). Additionally, the complete C-S-H gel chemical reactions cannot be homogeneously created across the matrix in the absence of water[112]. Water curing results in a higher C-S-H gel formation and a denser microstructure than air curing[113]. It was stated that AAS pastes cured in water up to 12 M exhibited higher compressive strength than their corresponding specimens cured in air[110]. Water can function as a solvent, enabling the reaction between slag particles and the activator. This process results in the creation of a gel-like substance, which is essential for strength gain. It was validated that AAS pastes cured in water for 28 days demonstrated higher compressive strength than those cured under alternative conditions. Similarly, AAS mortars soaked in water for up to 90 days[114], or slag/FA mortars immersed in water for up to 56 days[115] exhibited higher compressive strength than their references cured in air. The AAS mortars cured in water also demonstrated greater strength than those cured in a plastic cover[112]. It was confirmed that concretes made of AAS[116] or slag-$Ca(OH)_2$[113] immersed in water exhibited greater compressive strength compared to those cured in air.

To further emphasize the superior performance of water curing, Fig. 10 presents a comparison of compressive strengths under both curing methods at 28 days. The data reveal a robust linear relationship (R^2 = 0.99), confirming that the influence of BP on strength development is consistent across curing conditions. The figure visually reinforces that water curing consistently produces higher compressive strength than air curing, underscoring the critical role of sustained hydration in maximizing strength gain.

Environmental conditions

This test simulates real-world conditions that construction materials encounter, ensuring their relevance for evaluating their performance in actual building projects. This test primarily assesses the capacity of AAS pastes and those with different BP ratios to withstand environmental challenges linked to moisture. It indicates the mechanical strength, stability, and possible durability of the materials when applied in construction. Evaluating the performance of these materials in simulated scenarios provides valuable insights into their behaviour under real-world conditions. Figure 11 demonstrates how varying BP ratios influence the compressive strength of air

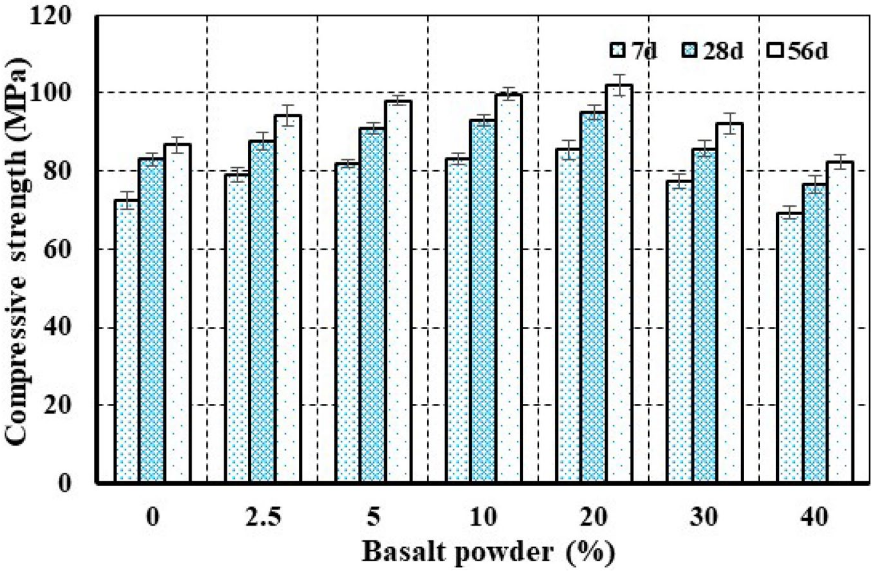

Fig. 9. Compressive strength changes with varying BP ratios for water cured specimens.

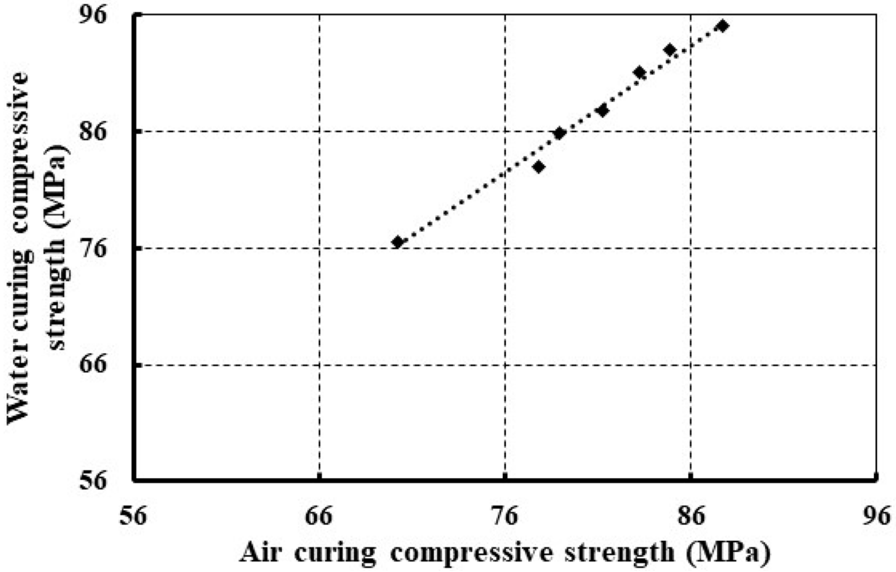

Fig. 10. Correlation between the 28-day compressive strength of air-cured and water-cured specimens.

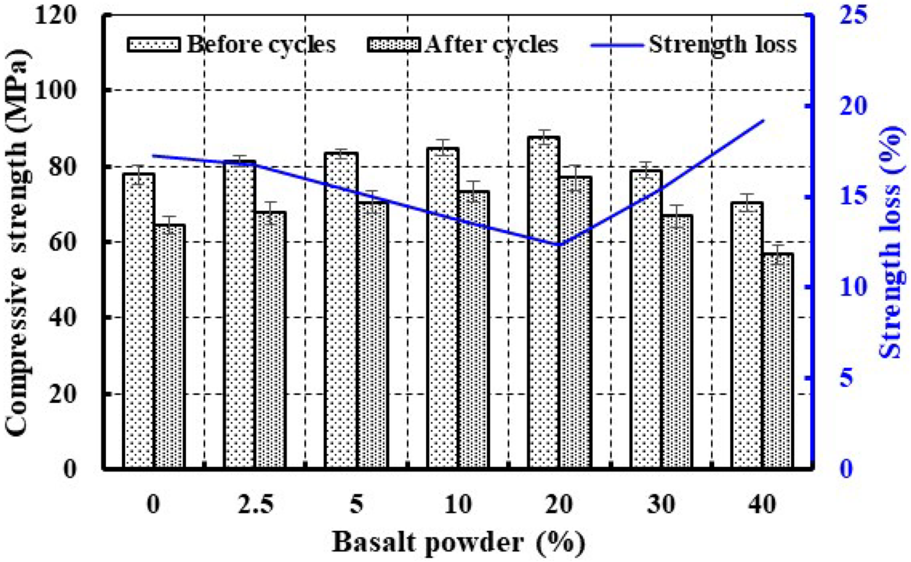

Fig. 11. Compressive strength and changes in strength loss with varying BP ratios for air cured specimens after 40 wetting/drying cycles.

cured specimens after undergoing 40 cycles of wetting-drying. Based on the visual evaluation, every specimen underwent the 40 cycles without any apparent failures occurring. As anticipated, following exposure, all specimens demonstrate a reduced compressive strength. This reduced strength may be relevant to the development of microcracks or increased porosity[117–119]. After cycles, 0B specimens show a 17.24% decrease in their original strength. This ratio gradually decreases with increasing BP up to 20%, then starts to increase. For instance, including BP at levels 2.5% (2.5B), 5% (5B), 10% (10B), and 20% (20B) shows 16.69%, 15.26%, 13.7%, and 12.32% decrease in the original strength, respectively. The results mean that repeated cycles cause degradation, but BP has a beneficial effect by slowing it down. The 20B specimens show the least degradation, confirming that 20% BP is the ideal ratio. Increasing BP to 30% (30B) results in an escalation in the strength loss from 12.32% for 20B to 15.36%, but still lower than 0B. The highest BP ratio (40%) adversely affects, causing a 19.16% increase in strength loss. The results of water curing specimens undergo 40 cycles of wetting-drying shown in Fig. 12, follow a similar trend, although the strength is higher and the strength loss is lower. For instance, after cycles, the 0B, 2.5B, 5B, 10B, 20B, 30B, and 40B show 7.74%, 6.74%, 5.83%, 4.57%, 3.63%, 7.19% and 11.63%, respectively, decrease in the original strength. These ratios are significantly lower than air curing specimens, confirming efficient water curing. The reasons for this positive influence are mentioned in Sect. Setting time.

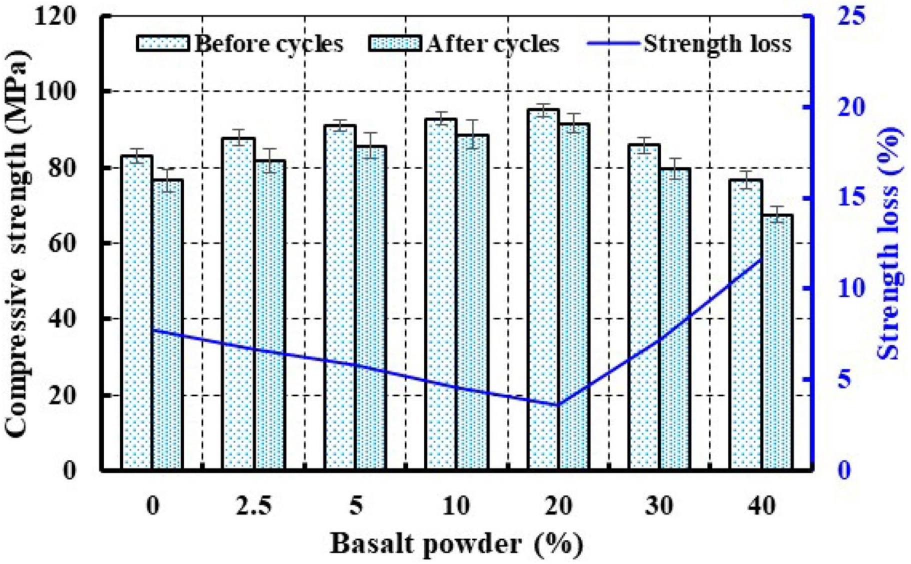

Fig. 12. Compressive strength and changes in strength loss with varying BP ratios for water cured specimens after 40 wetting/drying cycles.

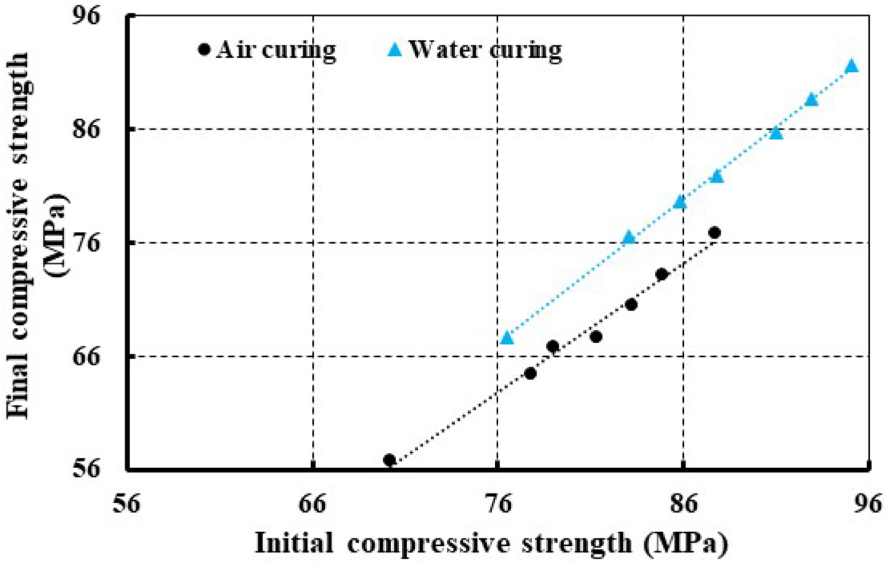

Fig. 13. Compressive strength after 40 wetting-drying cycles plotted against the initial 28-day strength for both air-cured and water-cured specimens.

The relationship between the initial 28-day strength and the final strength after 40 wetting-drying cycles is directly compared in Fig. 13. Two key observations can be made. First, for both curing methods, higher initial strength generally correlates with higher final strength. Second, and more importantly, the data series for the air-cured specimens falls significantly further below those of the water-cured series. This visually demonstrates the much greater performance degradation in the air-cured samples. The proximity of the water-cured data points provides powerful evidence of their superior durability and resistance to damage from environmental cycling, a finding that is consistent with the microstructural analysis.

Transport properties

Figure 14 demonstrates how varying BP ratios influence the transport properties of air cured specimens. The 0B specimens show 9.75% water absorption. This result falls below those declared in[120], whilst exceeding those listed in[112]. The 0B specimens show 20.24% porosity, which is higher than the result listed in[121] and lower than the result listed in[56]. Overall, the 0B transport properties are consistent with earlier studies. Including BP at levels 2.5% (2.5B), 5% (5B), 10% (10B), and 20% (20B) results in a beneficial influence on the transport properties. For instance, porosity drops to 19.5% (for 2.5B), 18.45% (for 5B), 17.38% (for 10B), and 16.25% (for 20B), whilst water absorption diminishes to 9.3% (for 2.5B), 8.8% (for 5B), 8.31% (for 10B), and 7.75% (for 20B). The incorporation of 20% BP results in the greatest reduction, meaning the greatest improvement. The outcomes strongly support the hypothesis that including BP in the pastes can effectively improve the microstructure and, subsequently, decrease transport properties. The reasons for this positive influence are discussed in Sect. Compressive strength. While including BP up to 20% was beneficial, further increases did not result in extra improvement. Instead, transport properties begin to deteriorate (increase), reaching their worst point when 40% BP was incorporated. This trend directly mirrors the compressive strength results and is explained by the same competing mechanisms. While up to 20% BP leads to pore refinement through a physical filler effect, higher replacement levels create what can be described as a 'binder-starved' system. As discussed in the literature[52], when the primary binder is excessively diluted, the resulting hydration products are insufficient to fill all the capillary pores. The resulting matrix is therefore inherently more porous and discontinuous, leading to interconnected pathways for water ingress and thus higher water absorption and porosity. The high reduction in the slag results in an insufficient amount of C-S-H (see Fig. 20b later) as well as increased SiO_2/Al_2O_3 ratios than the ideal. As a result, the microstructure becomes porous (see Figs. 21c and 22c later). The water curing specimens show a similar pattern of results to those of air curing, as presented in Fig. 15, but with a lower rate. This may be relevant to increased hydration products during water curing. This beneficial influence may be linked to the development of a compact matrix associated with smaller pore dimensions and reduced pore[116].

Drying shrinkage

As is known, excessive drying shrinkage poses a significant risk, frequently leading to damaging cracks that compromise the structural integrity and load-bearing ability of the material. This means that mitigating shrinkage results in higher strength and durability. Figure 16 demonstrates the drying shrinkage of 0B, 5B, 20B, and 40B specimens. Visually, the shrinkage appears to be influenced by the BP ratio and time. Across all specimens, a marked rapid shrinkage rate was observed throughout the first 16 days, followed by a somewhat slow rate. Unlike other studies showed that this rapid shrinkage occurred throughout the first 14 days[122]. The 0B specimens exhibit a notably high shrinkage rate[123]. A primary concern with AAS systems is their substantial shrinkage rate, which could pose a serious challenge to their effectiveness. The shrinkage of specimens may vary, either increasing or decreasing, depending on the BP ratio. Compared to 0B specimens, the specimens with 5% BP (5B), and 20% BP (20B) exhibit reduced shrinkage. The most significant decline in shrinkage rate was noted with including 20%. It is useful to state that conventional concrete, including 20% basalt fiber powder, can reduce the drying shrinkage[124]. The reduced shrinkage may be connected to the BP filler properties, which can occupy voids in the matrix and enhance packing. The BP ideal ratio can yield a denser microstructure, leading to a low-shrinkage paste. Contrarily, including 40% BP (40B) results in an increased shrinkage rate. This is ascribed to the formation of a porous microstructure and a weak matrix. It was reported that decreased porosity led to decreased drying shrinkage[125], in which the pore sizes can participate in the shrinkage[126].

Crystalline phases

Figure 17 shows the XRD patterns of 0B, 20B, and 40B samples cured in air. The 0B sample exhibits an amorphous phase. A distinct broad peak ranging from 25° to 35° 2θ indicates the presence of a grassy phase, predominantly composed of C-S-H gel. The semi-crystalline C-S-H gel phase, alongside calcite, can be detected[45]. Each of 20B and 40B exhibits a comparable amorphous phase, which is connected to the C-S-H gel (from slag) and N-A-

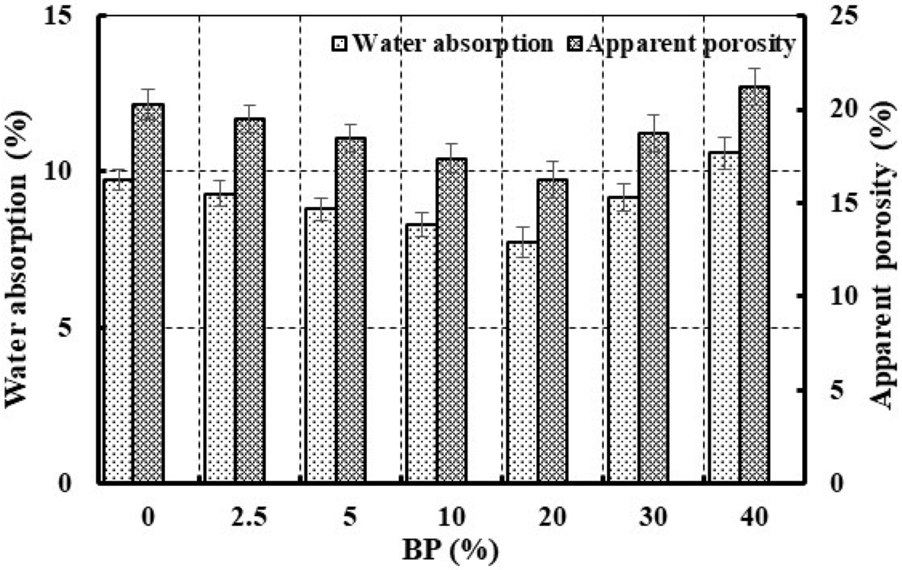

Fig. 14. Transport properties change with varying BP ratios for water cured specimens.

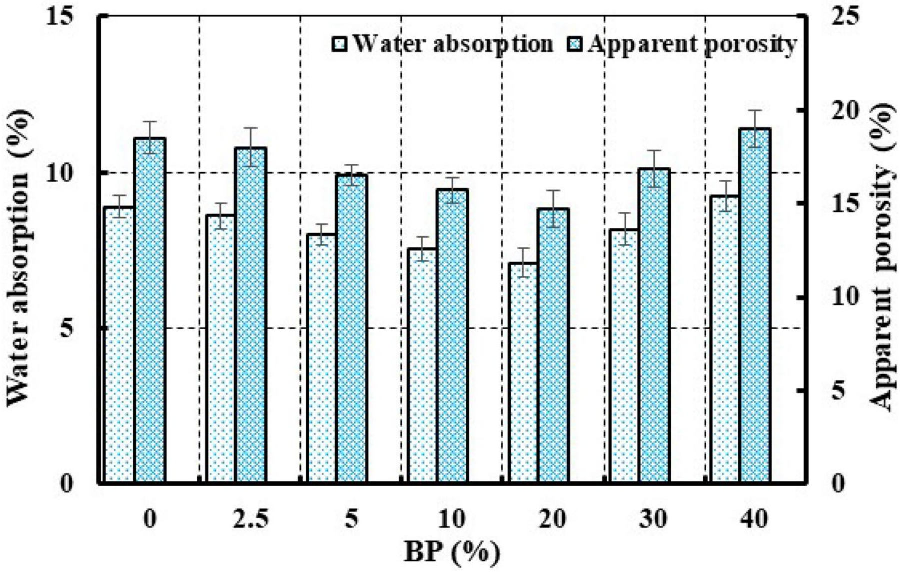

Fig. 15. Transport properties change with varying BP ratios for water cured specimens.

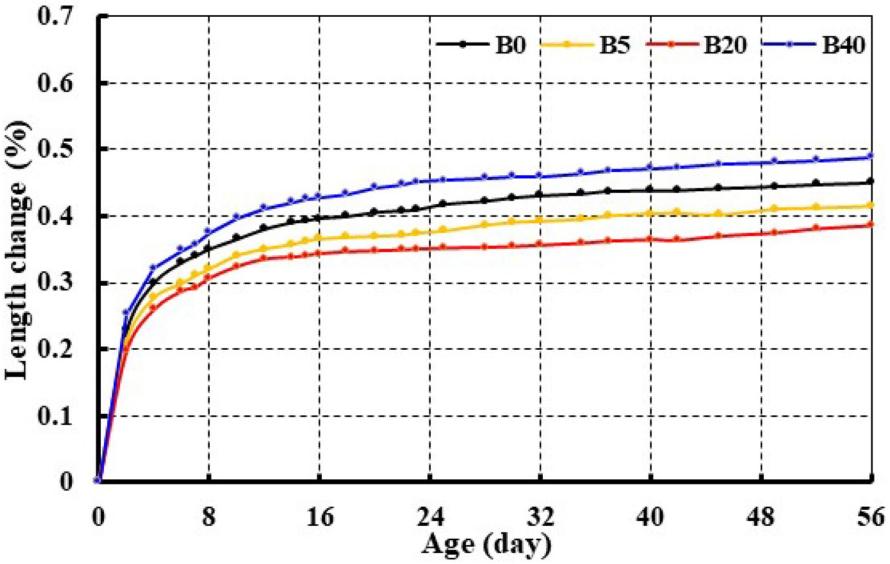

Fig. 16. Drying shrinkage changes with varying BP ratios.

S-H gel (from BP). The crystalline phases of diopside, anorthite, augite, albite, and calcite can also be detected. The intensity of these phases increases with increasing BP amount. Figure 18 shows the XRD patterns of 0B, 20B, and 40B samples cured in water. Similar amorphous humps to those cured in air were detected, but with higher intensities, which conform to their higher compressive strength. The crystalline phases in the samples cured in water are identical to those cured in air, but they have fewer peaks. This confirms that water curing has a significant effect on these phases than air curing. This emphasizes that specimens cured in water are stronger than those cured in air.

Thermogravimetric analysis

Figure 19 shows the TGA/DTG curves of the 0B sample cured in water. A unique endothermic peak below 200 ℃, along with a notable weight loss in TGA, was detected in the 0B sample. The former weight loss is linked to C-S-H gel's water evaporation[45]. This phase is responsible for material strength[127]. Poorly crystalline carbonate decomposition is linked to the small weight loss that is notable at 600–700 ℃[128]. Figure 20 shows the TGA/DTG curves of 20B and 40B samples cured in water. The analysis of these samples reveals greater weight losses between 600 and 700 ℃ compared to the 0B sample shown in Fig. 19. Compared to the 0B sample, a significant weight loss observed below 200 ℃ in 20B sample presented in Fig. 20a, which is associated with the coexistence

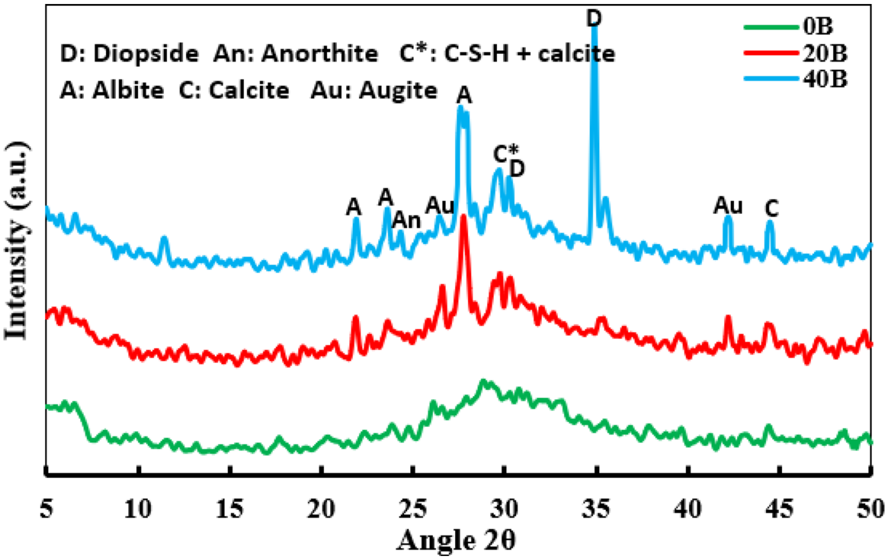

Fig. 17. Variation of XRD patterns with varying BP ratios for air cured samples.

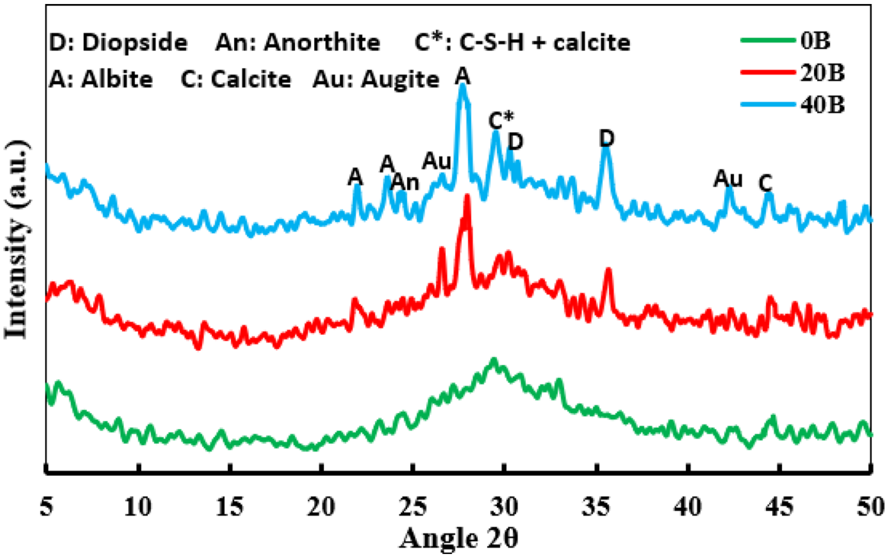

Fig. 18. Variation of XRD patterns with varying BP ratios for water cured samples.

of C-S-H gel form the primary slag source and N-A-S-H gel from adding BP. It was stated that introducing appropriate silica-rich material into slag enabled the formation of both C-S-H and N-A-S-H gel, contributing to microstructure density and improved strength[44]. This phenomenon of coexistence was observed in mixtures of slag with various low-calcium, silica-rich materials, including MK[40], FA/oil shale residue[129], volcanic glass powder[44], ceramic powder[46], FA[130], volcanic ash[131], and feldspar[104]. Strengthening is the result of this phase. This implies that better compressive strength results from greater weight loss[83]. Upon examining the weight loss data presented in Figs. 19 and 20, it becomes evident that the 20B sample (Fig. 20a) experiences the most significant weight loss, followed by the 0B sample (Fig. 19), whilst the 40B sample (Fig. 20b) demonstrates the least amount of weight loss. These findings corroborate the measured compressive strength trends demonstrated in Fig. 9.

Microstructure analysis

Figure 21 shows the SEM images of 0B, 20B, and 40B samples cured in air. The 0B sample is characterized by numerous partially reacted or nonreacted slag particles. These particles are easily distinguishable by their distinctive, irregular, and jagged shapes, which contrast with the surrounding material. Their bright gray color further emphasizes their presence. Moreover, this microstructure displays a scattered distribution of microcracks. It is hypothesized that high shrinkage in AAS matrices creates tension, leading to microcrack formation[132,133]. The microcrack formation is also hypothesized to stem from the volumetric variations associated with the

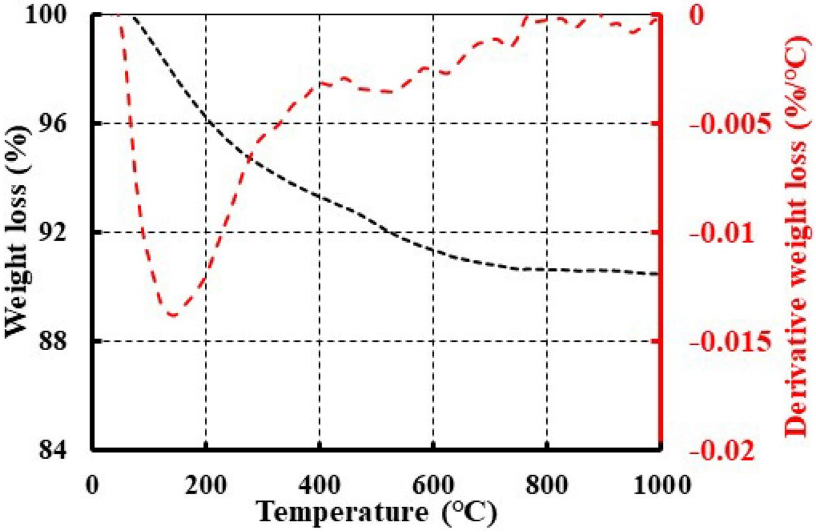

Fig. 19. TGA/DTG curves of 0B water cured sample.

transformation of the non-crystalline C-S-H phase into the semi-crystalline phase in incompletely solidified geopolymer gel[127]. It was theorized that the microcrack formation is associated with a greater uncombined water quantity that evaporated through drying[134]. Similar microcracks were found in other studies[135,136]. Including 20% BP (20B) dramatically transformed the microstructure compared to the sample presented in Fig. 21a. The microcracks vanished entirely and the microstructure abruptly altered into a more compact and denser, featuring only a limited number of unreacted particles and pores (Fig. 21b). This dense, visually homogenous matrix is the direct microstructural manifestation of the optimal synergy between the C-S-H gel from slag and the N-A-S-H gel from basalt, a co-existence suggested by our TGA and XRD results (Sect. Crystalline phases and 3.8). This observation aligns with the findings of Yip et al.[127], who described how the formation of co-existing C-S-H and geopolymeric gels can lead to superior particle packing and microstructural densification, which fully explains the enhanced mechanical and durability properties observed at the 20% BP replacement level. Accordingly, including 20% BP (20B) can enhance the microstructure compactness and prevent microcracks. This improved microstructure is the primary driver behind the observed enhanced strength (Figs. 8), reduced transport properties (Figs. 12), enhanced environmental resistance (Fig. 11), and reduced drying shrinkage (Fig. 16). The microcracks disappearance with including BP aligns with the hypothesis that specimens containing high calcium showed high shrinkage. However, including low calcium aluminosilicates in these specimens markedly decreased the shrinkage[137], thus mitigating the microcracks formation. Contrarily, the use of 40% BP (40B) leads to a different outcome: a porous microstructure with numerous numbers of nonreacted particles (Fig. 21c). These features are allied with the degradation of the 40B specimens' properties.

Figure 22 depicts the SEM images of 0B, 20B, and 40B samples treated in water. Despite the 0B sample treated in water exhibiting many nonreacted particles and some pores, it is free from microcracks (Fig. 22a). The disappearance of microcracks confirms the benefit of water curing in preventing microcracks[138]. Similar to 20B sample cured in air, including 20% BP (20B) can diminish the amount and dimensions of nonreacted particles, along with reducing the pore count as presented in Fig. 22b. This microstructure seems to not only surpass the 0B sample cured in water but also the 20B sample cured in air, shown in Fig. 21b. Introducing the greatest ratio of BP (i.e., 40%) promotes the formation of pores (Fig. 22c), which adversely affects compressive strength. Despite the formation of pores in the 40B sample cured in water, it still outperforms its counterpart cured in air shown in Fig. 21c.

Figure 23 shows the SEM images of 0B, 20B, and 40B samples cured in air after wetting-drying cycles. The 0B sample is characterized by microcracks as illustrated in Fig. 23a, which could have developed during the drying phase. These microcracks could provide pathways for ions and water to penetrate the sample upon wetting[139]. This alteration in the sample's microstructure is intricately connected to the strength degradation rate following cyclic exposure. The process of wetting-drying can lead to microcracks development, which weakens the strength[140]. Including 20% BP (20B) results in limiting the microcracks (Fig. 23b), which is positively reflected in its strength compared to 0B after exposure to the same number of cycles. This verifies that the ideal proportion of BP can enhance the microstructure and prevent strength loss. Contrarily, including 40% BP (40B) results in a porous microstructure and extensive microcracks (Fig. 23c), which is negatively reflected in its strength. Figure 24 shows the SEM images of 0B, 20B, and 40B samples cured in water after wetting-drying cycles. The trend of the microstructure of these samples is similar to their counterparts presented in Fig. 23, but with lower microstructure degradation due to water curing.

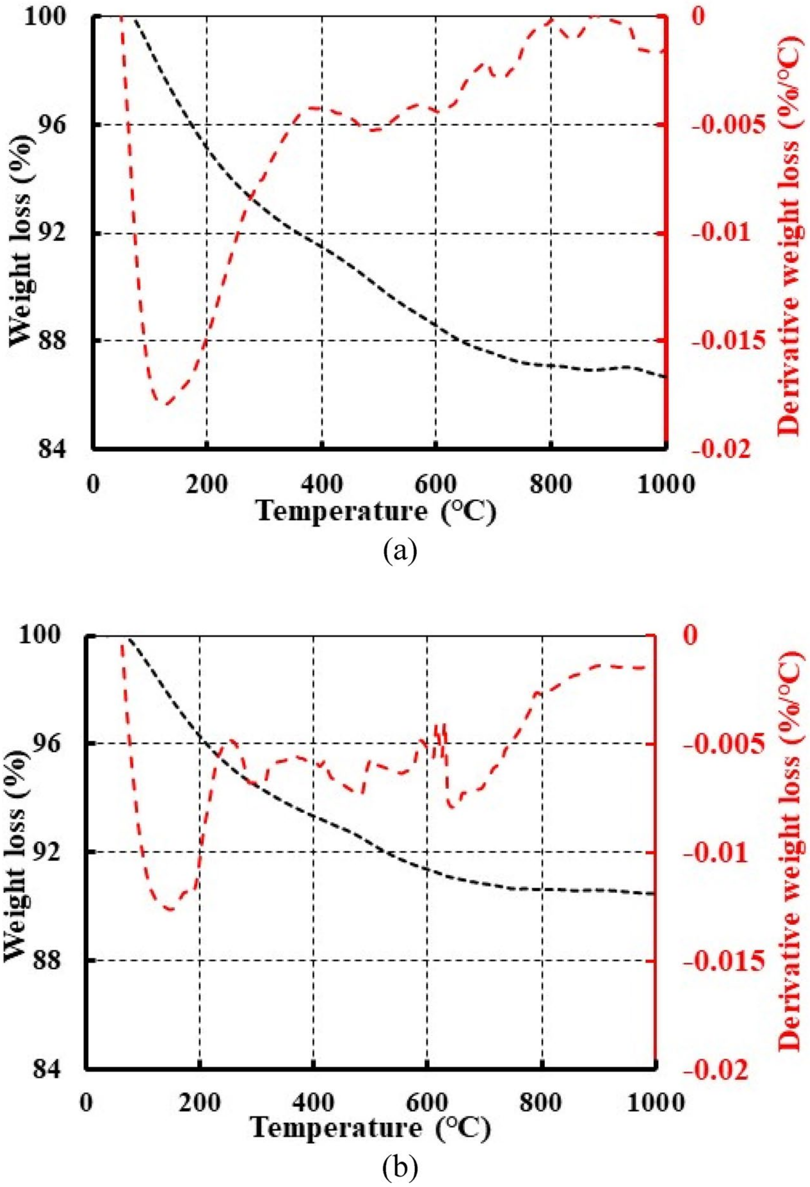

(a)

(b)

Fig. 20. TGA/DTG curves of 20B (**a**), and 40B (**b**) water cured samples.

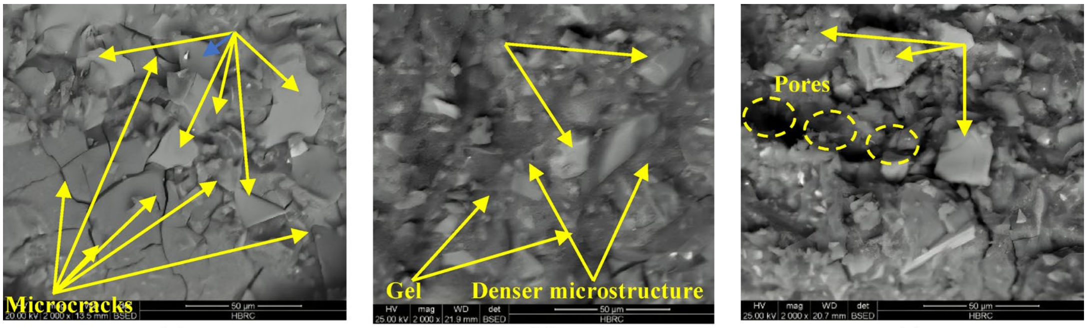

(a) (b) (c)

Fig. 21. SEM images of 0B (**a**), 20B (**b**), and 40B (**c**) samples cured in air.

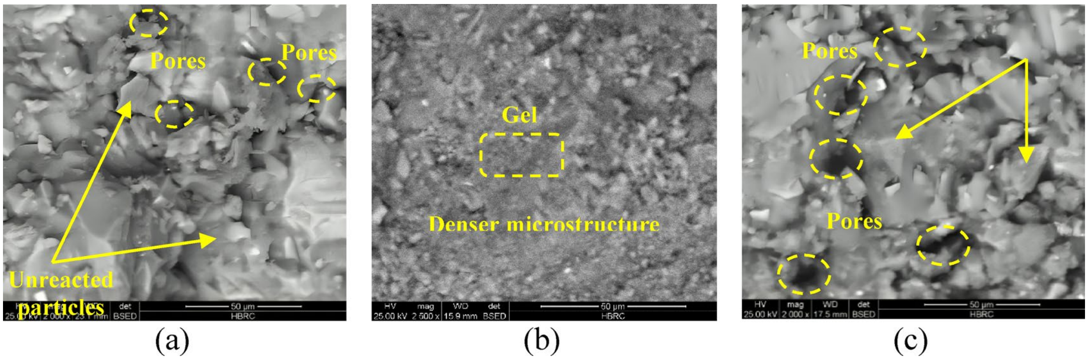

(a) (b) (c)

Fig. 22. SEM images of 0B (**a**), 20B (**b**), and 40B (**c**) samples cured in water.

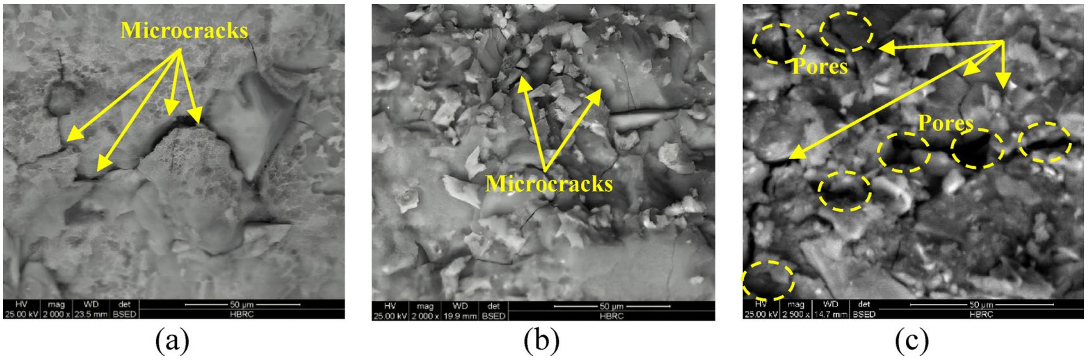

(a) (b) (c)

Fig. 23. SEM images of 0B (**a**), 20B (**b**), and 40B (**c**) samples cured in air after wetting-drying cycles.

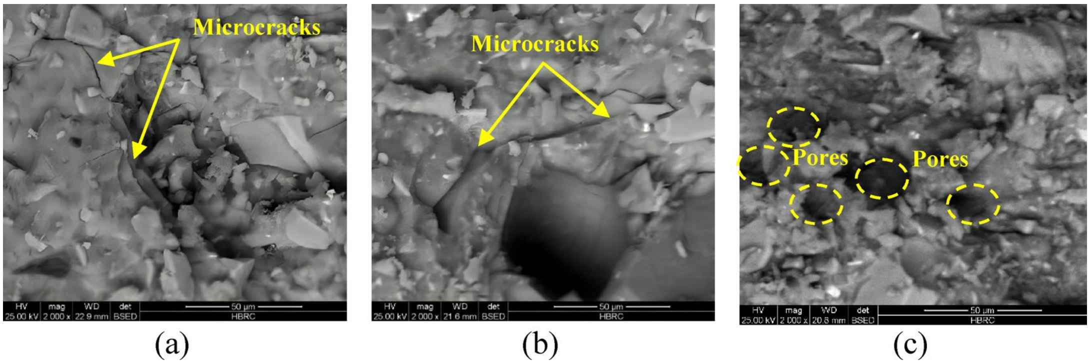

(a) (b) (c)

Fig. 24. SEM images of 0B (**a**), 20B (**b**), and 40B (**c**) samples cured in water after wetting-drying cycles.

Conclusions

This study addressed a critical research gap concerning the enhancement of AAS cement using widely available natural materials. It provides the first comprehensive evidence that Egyptian BP can serve as an effective fortifier, not merely a filler, for AAS systems. The central conclusion is that a specific, optimal replacement of 20% BP leads to a synergistic improvement in mechanical strength, transport properties, and environmental durability. This enhancement is driven by the formation of a densified, co-existing C-S-H and N-A-S-H gel matrix, which overcomes the potential performance loss from diluting the primary slag binder. Furthermore, the study confirms the critical role of water curing in mitigating microcracks and maximizing the binder's long-term durability. The specific findings that support these overarching conclusions are summarized as follows:

1. The proper application of BP can optimize AAS cement properties.
2. Adding BP slightly decreased the mixture's flowability due to its finer particles than slag.
3. Adding BP prolonged the setting time due to the increased silica in BP at the expense of calcium in slag.

4. Adding 0.5–20% BP improved the compressive strength, as high as 14.54% at 28 days and 17.65% at 90 days under water curing, due to the filling effect of fine BP and the formation of N-A-S-H gel that can exist alongside C-S-H gel.
5. Adding 20% BP improved the material's performance in harsh environmental conditions, significantly reducing the strength degradation to 3.63% even after 40 repeated wetting-drying cycles.
6. Adding 0.5–20% BP decreased transport properties by blocking the pores and densifying the microstructure.
7. Adding 5% and 20% BP mitigated the drying shrinkage, due to the packing effect, whilst adding 40% BP caused negative consequences owing to the formation of pores.
8. Generally, adding 20% BP showed the ideal ratio. However, adding 30% BP showed only a marginal effect, whilst adding 40% BP had a detrimental effect on the overall properties of cement.
9. Water curing showed superiority over air curing in this cement type by inhibiting the development of microcracks and facilitating the C-S-H gel formation.

While this study successfully identified key performance trends, further research is needed for practical application. Its limitations should be acknowledged to provide context for its findings. These include its focus on a single source of basalt and slag, whose specific mineralogical and chemical properties may influence the outcomes. Additionally, the durability assessment was confined to physical wetting-drying cycles, which do not cover the full spectrum of potential environmental exposures such as chemical attack or freeze-thaw conditions. Building on these findings, future research is needed for practical application. A future optimization study should be conducted, focusing on the most promising formulations (i.e., those with 10–20% BP). This next phase of research should employ a statistical Design of Experiments (DoE) to investigate the interplay between basalt powder content, activator concentration, and curing conditions. The use of Analysis of Variance (ANOVA) will be essential to statistically validate the results and develop a robust, optimized mix design. Furthermore, to address the current limitations, future work should expand to include basalts from different geological origins and evaluate long-term durability under aggressive chemical environments (e.g., sulfate and chloride exposure), which would provide a more complete and universally applicable picture of the material's service life.

Data availability

All data, models, and code generated or used during the study appear in the submitted article.

Received: 16 April 2025; Accepted: 9 September 2025

References

1. Wu, Y. et al. Geopolymer, green alkali activated cementitious material: synthesis, applications and challenges. *Constr. Build. Mater.* **224**, 930–949 (2019).
2. Snellings, R. Assessing, Understanding and unlocking supplementary cementitious materials. *RILEM Tech. Lett.* **1**, 50–55 (2016).
3. Singh, V. K. The Science and Technology of Cement and Other Hydraulic Binders, Elsevier2023.
4. Rice, M. B., Thurston, G. D., Balmes, J. R. & Pinkerton, K. E. Climate change. A global threat to cardiopulmonary health. *Am. J. Respir. Crit Care Med.* **189** (5), 512–519 (2014).
5. Hossain, S. S. & Akhtar, F. Recent progress of geopolymers for carbon dioxide capture, storage and conversion. *J. CO2 Utilization*. **78**, 102631 (2023).
6. Özkan, S. & Acaralı, N. Efficiency enhancement and cost reduction in cement clinker production: A comprehensive energy and exergy analysis of a rotary kiln in Turkey. *Therm. Sci. Eng. Progress*. **53**, 102744 (2024).
7. Thai, T., Kučera, P. & Bernatik, A. Noise pollution and its correlations with occupational noise-induced hearing loss in cement plants in Vietnam. *Int. J. Environ. Res. Public Health*. **18** (8), 4229 (2021).
8. Meeus, L. Appraisal of the European commission's energy roadmap 2050. *Eur. Energy Clim. J.* **2** (2), 48–56 (2012).
9. Rashad, A. M. A brief on high-volume class F fly Ash as cement replacement–A guide for civil engineer. *Int. J. Sustainable Built Environ.* **4** (2), 278–306 (2015).
10. Rashad, A. M. An overview of pumice stone as a cementitious material–the best manual for civil engineer. *Silicon* **13** (2), 551–572 (2021).
11. Rashad, A. M. Metakaolin as cementitious material: history, scours, production and composition–A comprehensive overview. *Constr. Build. Mater.* **41**, 303–318 (2013).
12. Rashad, A. M., Essa, G. M., Mossalam, E. A. & Mohamed, R. A. E. Enhancing water resistance, improving corrosion behavior, and modifying properties of Metakaolin geopolymer cement with trisodium citrate. *J. Building Eng.* 113812. (2025).
13. Rashad, A. M. An overview on rheology, mechanical properties and durability of high-volume slag used as a cement replacement in paste, mortar and concrete. *Constr. Build. Mater.* **187**, 89–117 (2018).
14. Pacheco-Torgal, F., Labrincha, J., Leonelli, C., Palomo, A. & Chindaprasit, P. *Handbook of alkali-activated Cements, Mortars and Concretes* (Elsevier, 2014).
15. Rashad, A. M., Mohamed, R. A. E., Zeedan, S. R. & El-Gamal, A. Basalt powder as a promising candidate material for improving the properties of fly Ash geopolymer cement. *Constr. Build. Mater.* **435**, 136805 (2024).
16. Gharieb, M. & Rashad, A. M. A pioneer investigation on recycling ceramic sludge waste into Alkali-Activated slag cement. *Arab. J. Sci. Eng.* 1–14. (2025).
17. Gharieb, M. & Rashad, A. M. Impact of sugar beet waste on strength and durability of Alkali-Activated slag cement. *ACI Mater. J.* **119**(2) (2022).
18. Taylor, H. F. Cement chemistry, Thomas Telford London (1997).
19. Mehta, P. K. & Monteiro, P. J. *Concrete: Microstructure, Properties, and Materials* (McGraw-Hill Education, 2014).
20. Rashad, A. M. A comprehensive overview about the influence of different admixtures and additives on the properties of alkali-activated fly Ash. *Mater. Design*. **53**, 1005–1025 (2014).
21. Qaidi, S. M. et al. Recycling of mine tailings for the geopolymers production: A systematic review. *Case Stud. Constr. Mater.* **16**, e00933 (2022).
22. Rashad, A. M. A comprehensive overview about the influence of different additives on the properties of alkali-activated slag–A guide for civil engineer. *Constr. Build. Mater.* **47**, 29–55 (2013).
23. Rashad, A. M., Mosleh, Y. A. & Mokhtar, M. Thermal insulation and durability of alkali-activated lightweight slag mortar modified with silica fume and fly Ash. *Constr. Build. Mater.* **411**, 134255 (2024).

24. Samadhiya, A., Bhunia, D., Chakraborty, S. & Lahoti, M. Influence of activator ratios and concentration on the physio-mechanical and microstructural characteristics of the geopolymers derived from sandstone processing waste. *Environ. Sci. Pollut. Res.* 1–16. (2024).
25. Kaya, M. et al. The effect of marble powder on physico-mechanical and microstructural properties of kaolin-based geopolymer pastes. *Struct. Concrete*. **24** (5), 6485–6504 (2023).
26. Zareechian, M., Siad, H., Lachemi, M. & Sahmaran, M. Advancements in cleaner production of one-part geopolymers: A comprehensive review of mechanical properties, durability, and microstructure. *Constr. Build. Mater.* **409**, 133876 (2023).
27. Amran, Y. M., Alyousef, R., Alabduljabbar, H. & El-Zeadani, M. Clean production and properties of geopolymer concrete; A review. *J. Clean. Prod.* **251**, 119679 (2020).
28. Rashad, A. M. Alkali-activated metakaolin: A short guide for civil Engineer–An overview. *Constr. Build. Mater.* **41**, 751–765 (2013).
29. Rashad, A. M. Behavior of steel slag aggregate in mortar and concrete-A comprehensive overview. *J. Building Eng.* **53**, 104536 (2022).
30. Rashad, A. M. A synopsis manual about recycling steel slag as a cementitious material. *J. Mater. Res. Technol.* **8** (5), 4940–4955 (2019).
31. Rashad, A. M., Khafaga, S. A. & Gharieb, M. Valorization of fly Ash as an additive for electric Arc furnace slag geopolymer cement. *Constr. Build. Mater.* **294**, 123570 (2021).
32. Kuehl, H. Slag cement and process of making the same, Google Patents, (1908).
33. Rashad, A. M. Silica fume in geopolymers: A comprehensive review of its effects on properties. *SpringerBriefs Appl. Sci. Technol.* https://doi.org/10.1007/978-3-031-33219-7 (2023).
34. Rashad, A. M. The effect of polypropylene, polyvinyl-alcohol, carbon and glass fibres on geopolymers properties. *Mater. Sci. Technol.* **35** (2), 127–146 (2019).
35. Rashad, A. M. Effect of steel fibers on geopolymer properties–The best synopsis for civil engineer. *Constr. Build. Mater.* **246**, 118534 (2020).
36. Amran, M. et al. Fiber-reinforced alkali-activated concrete: A review. *J. Building Eng.* **45**, 103638 (2022).
37. Rashad, A. M., Mohamed, H., Khalil, M. H., Hammed, H. & El-Gamal, A. Effect of micro-sized lead oxide on the workability, mechanical strength and durability of alkali-activated slag mortar. *Constr. Build. Mater.* **373**, 130890 (2023).
38. Rashad, A. M. Effect of nanoparticles on the properties of geopolymer materials. *Magazine Concrete Res.* **71** (24), 1283–1301 (2019).
39. Rashad, A. M. Calcium hydroxide in geopolymers–a critical overview. *Eur. J. Environ. Civil Eng.* 1–29. (2024).
40. Rashad, A. M. Metakaolin effect on geopolymers' properties. *SpringerBriefs Appl. Sci. Technol.* https://doi.org/10.1007/978-3-031-45151-5 (2024).
41. Rashad, A. M. Effect of limestone powder on the properties of alkali-activated materials–A critical overview. *Constr. Build. Mater.* **356**, 129188 (2022).
42. Rashad, A. M., Mosleh, Y. A. & Gharieb, M. Preparatory study about effect of feldspar on properties of Alkali-activated slag concrete. *ACI Mater. J.* **120** (2), 53–63 (2023).
43. Rashad, A. M. A concise on the effect of calcium oxide on the properties of Alkali-Activated materials: A manual for civil engineers. *Int. J. Concrete Struct. Mater.* **17** (1), 72 (2023).
44. Rashad, A. M., Abdu, M. F. A. & Ezzat, M. Egyptian volcanic glass powder as a modifier agent for alkali-activated slag cement. *Constr. Build. Mater.* **408**, 133662 (2023).
45. Rashad, A. M., Mokhtar, M., El-Nashar, M. & Mohamed, R. A. E. Waste marble powder emerges as a promising material choice to enhance the properties of alkali-activated slag cement. *Sustainable Chem. Pharm.* **43**, 101864 (2025).
46. Rashad, A. M. & Essa, G. M. Effect of ceramic waste powder on alkali-activated slag pastes cured in hot weather after exposure to elevated temperature. *Cem. Concr. Compos.* **111**, 103617 (2020).
47. Staff, U. USGS mineral review.
48. Robayo-Salazar, R. A. & de Gutiérrez, R. M. Natural volcanic Pozzolans as an available Raw material for alkali-activated materials in the foreseeable future: A review. *Constr. Build. Mater.* **189**, 109–118 (2018).
49. Wang, W., Noguchi, T., Tomoyose, A., Zhang, Y. & Maruyama, I. Influence of volcanic glass powder on alkali-silica reaction expansion in alkali-activated slag mortars. *Cem. Concr. Compos.* **152**, 105665 (2024).
50. Miraki, H. et al. Clayey soil stabilization using alkali-activated volcanic Ash and slag. *J. Rock Mech. Geotech. Eng.* **14** (2), 576–591 (2022).
51. Rashad, A. M. & Abdu, M. F. A. Accelerated aging resistance, abrasion resistance and other properties of alkali-activated slag mortars containing limestone powder. *Sustainable Chem. Pharm.* **37**, 101406 (2024).
52. Rashad, A. M., Morsi, W. & Khafaga, S. A. Effect of limestone powder on mechanical strength, durability and drying shrinkage of alkali-activated slag pastes. *Innovative Infrastructure Solutions*. **6** (2), 127 (2021).
53. Robayo-Salazar, R. A., de Gutiérrez, M. & Puertas, F. Study of synergy between a natural volcanic Pozzolan and a granulated blast furnace slag in the production of geopolymeric pastes and mortars. *Constr. Build. Mater.* **157**, 151–160 (2017).
54. Rashad, A. M. An exploratory study on alkali-activated slag blended with quartz powder under the effect of thermal Cyclic loads and thermal shock cycles. *Constr. Build. Mater.* **70**, 165–174 (2014).
55. Rashad, A. M., Zeedan, S. R. & Hassan, H. A. A preliminary study of autoclaved alkali-activated slag blended with quartz powder. *Constr. Build. Mater.* **33**, 70–77 (2012).
56. Al-kroom, H., Al-Jabri, K., Tawfik, T. A., Abdel-Gawwad, H. A. & Rashad, A. M. Investigating the promising effect of thermally-treated Talc powder on the performance of alkali-activated slag cement. *Innovative Infrastructure Solutions*. **9** (8), 298 (2024).
57. Jamshaid, H. & Mishra, R. A green material from rock: basalt fiber–a review. *J. Text. Inst.* **107** (7), 923–937 (2016).
58. Perevozchikova, B., Pisciotta, A., Osovetsky, B., Menshikov, E. & Kazymov, K. Quality evaluation of the Kuluevskaya basalt outcrop for the production of mineral fiber, Southern urals. *Russia Energy Procedia*. **59**, 309–314 (2014).
59. Yang, W. et al. A review of the mechanical properties and durability of basalt fiber recycled concrete. *Constr. Build. Mater.* **412**, 134882 (2024).
60. Zheng, Y., Zhang, Y., Zhuo, J., Zhang, Y. & Wan, C. A review of the mechanical properties and durability of basalt fiber-reinforced concrete. *Constr. Build. Mater.* **359**, 129360 (2022).
61. Li, Y. et al. A review on durability of basalt fiber reinforced concrete. *Compos. Sci. Technol.* **225**, 109519 (2022).
62. Rashad, A. M. A synopsis about the effect of basalt and natural fibers on geopolymer properties. *Nat. Resour. Conserv. Res.* **1**(1) (2018).
63. Boğa, A. R. & Şenol, A. F. The effect of waste marble and basalt aggregates on the fresh and hardened properties of high strength self-compacting concrete. *Constr. Build. Mater.* **363**, 129715 (2023).
64. Scheinherrova, L., Keppert, M. & Černý, R. Chemical aspects of the application of basalt in cement composites. *Constr. Build. Mater.* **350**, 128873 (2022).
65. Ponzi, G. G. D. et al. Basalt powder as a supplementary cementitious material in cement paste for CCS wells: chemical and mechanical resistance of cement formulations for CO2 geological storage sites. *Int. J. Greenhouse Gas Control*. **109**, 103337 (2021).
66. Gheller, R., Silva, L. L., Fiori, M. A. & Batiston, E. R. Exploratory study for the alkaline activation of basalt powder as a supplementary cementitious matrix. *Revista IBRACON De Estruturas E Materiais*. **15**, e15405 (2022).

67. Lei, S. et al. Characteristics of lightweight geopolymers from microwave curing of basalt and waste glass powder mixtures. *Constr. Build. Mater.* **409**, 133758 (2023).
68. Akturk, B. & Ayhan, B. U. Alkali-activated basalt powder/slag systems: compressive strength and microstructural characterization. *Mater. Struct.* **56** (4), 81 (2023).
69. Akturk, B. Fracture behavior of alkali-activated basalt powder/slag systems reinforced with basalt and hybrid fibers. *Mater. Struct.* **56** (2), 46 (2023).
70. Dener, M. Mechanical and durability properties of alkali-activated slag/waste basalt powder mixtures, Proceedings of the Institution of Mechanical Engineers, Part L: Journal of Materials: Design and Applications 237(10) 2250–2265. (2023).
71. Moghazi, A. K. M. Geochemistry of a tertiary continental basalt suite, red sea coastal plain, egypt: petrogenesis and characteristics of the mantle source region. *Geol. Mag.* **140** (1), 11–24 (2003).
72. Bosworth, W. Geological evolution of the Red Sea: historical background, review, and synthesis, The Red Sea: The formation, morphology, oceanography and environment of a young ocean basin 45–78. (2015).
73. Mostafa, M., Afify, N., Gaber, A. & Abu Zaid, E. Investigation of thermal properties of some basalt samples in Egypt. *J. Therm. Anal. Calorim.* **75** (1), 179–188 (2004).
74. Aal, A. A. Mineral and chemical composition of basalts in the neighbourhood of giza, Egypt. *J. Afr. Earth Sc.* **26** (1), 101–117 (1998).
75. Mallory-Greenough, L. M., Greenough, J. D. & Owen, J. V. The stone source of predynastic basalt vessels: mineralogical evidence for quarries in Northern Egypt. *J. Archaeol. Sci.* **26** (10), 1261–1272 (1999).
76. Rashad, A. M. & Refaie, F. A. Z. Valuation of amorphous and crystalline phases of natural materials as modifier agents for High-Volume slag cement. *Arab. J. Sci. Eng.* 1–19. (2024).
77. Mao, Q., Li, Y., Liu, K., Peng, H. & Shi, X. Mechanism, characterization and factors of reaction between basalt and alkali: exploratory investigation for potential application in geopolymer concrete. *Cem. Concr. Compos.* **130**, 104526 (2022).
78. González-Ortega, M. A., Cavalaro, S., de Sensale, G. R. & Aguado, A. Durability of concrete with electric Arc furnace slag aggregate. *Constr. Build. Mater.* **217**, 543–556 (2019).
79. Yang, Y., Yang, E. H. & Li, V. C. Autogenous healing of engineered cementitious composites at early age. *Cem. Concr. Res.* **41** (2), 176–183 (2011).
80. Rashad, A. M. Influence of different additives on the properties of sodium sulfate activated slag. *Constr. Build. Mater.* **79**, 379–389 (2015).
81. Rashad, A. M., Morsi, W. & Khafaga, S. A. Effect of limestone powder on mechanical strength, durability and drying shrinkage of alkali-activated slag pastes. *Innovative Infrastructure Solutions*. **6** (2), 1–12 (2021).
82. Rashad, A. M., Zeedan, S. R. & Gharieb, M. Appreciation of sugar beet waste in Metakaolin geopolymer mortar for compressive strength and drying shrinkage. *Sustainable Chem. Pharm.* **37**, 101429 (2024).
83. Rashad, A. M., Essa, G. M., Morsi, W. & Fahmy, E. Calcium nitrate as a modifier agent for metakaolin-based geopolymer mortar. *Constr. Build. Mater.* **456**, 139199 (2024).
84. Rashad, A. M. & Sadek, D. M. An exploratory study on alkali-activated slag blended with microsize Metakaolin particles under the effect of seawater attack and tidal zone. *Arab. J. Sci. Eng.* **47** (4), 4499–4510 (2022).
85. Rashad, A. M., Sadek, D. M. & Gharieb, M. Valorization of quartz powder for drying shrinkage and carbonation resistance of alkali-activated slag cement. *Environ. Sci. Pollut. Res.* **29** (30), 45191–45203 (2022).
86. Tennakoon, C., San Nicolas, R., Sanjayan, J. G. & Shayan, A. Thermal effects of activators on the setting time and rate of workability loss of geopolymers. *Ceram. Int.* **42** (16), 19257–19268 (2016).
87. Sun, R. et al. Effect of white mud on properties of alkali activated slag. *Constr. Build. Mater.* **392**, 131944 (2023).
88. Rashad, A. M. & Ezzat, M. A preliminary study on the use of magnetic, zamzam, and sea water as mixing water for alkali-activated slag pastes. *Constr. Build. Mater.* **207**, 672–678 (2019).
89. Rashad, A. M., Eessaa, A. K., Khalil, M. H. & Mohamed, O. An initial study on the effect of nano-zirconium on the behavious of alkali-activated slag cement subjected to seawater attack. *Constr. Build. Mater.* **370**, 130659 (2023).
90. Zhu, X. et al. Chemical and physical effects of high-volume limestone powder on sodium silicate-activated slag cement (AASC). *Constr. Build. Mater.* **292**, 123257 (2021).
91. Zhang, B. et al. Improving the high temperature resistance of alkali-activated slag paste using municipal solid waste incineration bottom Ash. *J. Building Eng.* **72**, 106664 (2023).
92. Shen, M. et al. Effects of basalt powder and silica fume on ultra-high-strength cementitious matrix: A comparative study. *Case Stud. Constr. Mater.* **17**, e01397 (2022).
93. Scherer, C., de Lima, L. F. & Zorzi, J. E. Effect of partial replacement of cement by fine powders on the corrosion resistance of concrete. *Constr. Build. Mater.* **401**, 132982 (2023).
94. Liu, C., Yao, X. & Zhang, W. Controlling the setting times of one-part alkali-activated slag by using honeycomb ceramics as carrier of sodium silicate activator. *Constr. Build. Mater.* **235**, 117091 (2020).
95. Dung, N. T., Chang, T. P. & Chen, C. T. Engineering and sulfate resistance properties of slag-CFBC fly Ash paste and mortar. *Constr. Build. Mater.* **63**, 40–48 (2014).
96. Sun, B., Sun, Y., Ye, G. & De Schutter, G. A mix design methodology of slag and fly ash-based alkali-activated paste. *Cem. Concr. Compos.* **126**, 104368 (2022).
97. Javed, U., Shaikh, F. U. A. & Sarker, P. K. Microstructural investigation of lithium slag geopolymer pastes containing silica fume and fly Ash as additive chemical modifiers. *Cem. Concr. Compos.* **134**, 104736 (2022).
98. Lemougna, P. N. et al. Effect of slag on the improvement of setting time and compressive strength of low reactive volcanic Ash geopolymers synthetized at room temperature. *Mater. Chem. Phys.* **239**, 122077 (2020).
99. Wetzel, A. & Middendorf, B. Influence of silica fume on properties of fresh and hardened ultra-high performance concrete based on alkali-activated slag. *Cem. Concr. Compos.* **100**, 53–59 (2019).
100. Venyite, P. et al. Effect of combined Metakaolin and basalt powder additions to laterite-based geopolymers activated by rice husk Ash (RHA)/NaOH solution. *SILICON* **14**, 1643–1662 (2022).
101. Laibao, L., Yunsheng, Z., Wenhua, Z., Zhiyong, L. & Lihua, Z. Investigating the influence of basalt as mineral admixture on hydration and microstructure formation mechanism of cement. *Constr. Build. Mater.* **48**, 434–440 (2013).
102. Li, Z., Nedeljković, M., Chen, B. & Ye, G. Mitigating the autogenous shrinkage of alkali-activated slag by Metakaolin. *Cem. Concr. Res.* **122**, 30–41 (2019).
103. Ju, C. et al. Effect of calcium oxide on mechanical properties and microstructure of alkali-activated slag composites at sub-zero temperature. *J. Building Eng.* 101561. (2020).
104. Rashad, A. M., Mosleh, Y. A. & Gharieb, M. Preparatory study about effect of feldspar on properties of Alkali-Activated slag concrete. *ACI Mater. J.* **120**(2) (2023).
105. Riahi, S., Nemati, A., Khodabandeh, A. & Baghshahi, S. The effect of mixing molar ratios and sand particles on microstructure and mechanical properties of metakaolin-based geopolymers. *Mater. Chem. Phys.* **240**, 122223 (2020).
106. Khale, D. & Chaudhary, R. Mechanism of geopolymerization and factors influencing its development: a review. *J. Mater. Sci.* **42**, 729–746 (2007).
107. Rashad, A. M. & Zeedan, S. R. Effect of silica fume and activator concentration on Metakaolin geopolymer exposed to thermal loads. *Mater. J.* (2022).

108. Sun, Q., Li, T. & Liang, B. Preparation of a new type of cemented paste backfill with an alkali-activated silica fume and slag composite binder. *Materials* **13** (2), 372 (2020).
109. Liu, Y., Shi, C., Zhang, Z., Li, N. & Shi, D. Mechanical and fracture properties of ultra-high performance geopolymer concrete: effects of steel fiber and silica fume. *Cem. Concr. Compos.* 103665. (2020).
110. Rashad, A. M. & Mosleh, Y. A. Effect of tidal zone and seawater attack on Alkali-Activated blended slag pastes. *ACI Mater. J.* **119**(2) (2022).
111. Rashad, A. M. & Ouda, A. S. Effect of tidal zone and seawater attack on high-volume fly Ash pastes enhanced with Metakaolin and quartz powder in the marine environment. *Microporous Mesoporous Mater.* **324**, 111261 (2021).
112. Rostami, M. & Behfarnia, K. The effect of silica fume on durability of alkali activated slag concrete. *Constr. Build. Mater.* **134**, 262–268 (2017).
113. Yang, K. H., Cho, A. R., Song, J. K. & Nam, S. H. Hydration products and strength development of calcium hydroxide-based alkali-activated slag mortars. *Constr. Build. Mater.* **29**, 410–419 (2012).
114. Karim, M. R., Hossain, M. M., Elahi, M. M. A. & Zain, M. F. M. Effects of source materials, fineness and curing methods on the strength development of alkali-activated binder. *J. Building Eng.* **29**, 101147 (2020).
115. Dong, M., Elchalakani, M. & Karrech, A. Curing conditions of Alkali-Activated fly Ash and slag mortar. *J. Mater. Civ. Eng.* **32** (6), 04020122 (2020).
116. El-Hassan, H., Shehab, E. & Al-Sallamin, A. Influence of different curing regimes on the performance and microstructure of alkali-activated slag concrete. *J. Mater. Civ. Eng.* **30** (9), 04018230 (2018).
117. Rashad, A. M., Gharieb, M., Shoukry, H. & Mokhtar, M. Valorization of sugar beet waste as a foaming agent for Metakaolin geopolymer activated with phosphoric acid. *Constr. Build. Mater.* **344**, 128240 (2022).
118. Mohamed, H., El-Gamal, A., Khalil, M. H., Hammed, H. & Rashad, A. M. Valorization of nano-PbO as an additive to modify the properties and radiation shielding of alkali-activated slag mortar. *Mater. Chem. Phys.* **287**, 126277 (2022).
119. Gharieb, M. & Rashad, A. M. Impact of sugar beet waste on strength and durability of Alkali-Activated slag cement. *Mater. J.* **119** (2), 79–90 (2022).
120. Billong, N., Oti, J. & Kinuthia, J. Using silica fume based activator in sustainable geopolymer binder for Building application. *Constr. Build. Mater.* **275**, 122177 (2021).
121. Danish, A. et al. Performance evaluation and cost analysis of prepacked geopolymers containing waste marble powder under different curing temperatures for sustainable built environment. *Resour. Conserv. Recycl.* **192**, 106910 (2023).
122. Xu, R., Kong, F., Yang, R., Wang, H. & Hong, T. Drying shrinkage mitigation of alkali-activated blast furnace slag-copper slag by polyether-based shrinkage reducing admixture and MgO-based expansion agent. *Constr. Build. Mater.* **416**, 135172 (2024).
123. Mastali, M., Kinnunen, P., Dalvand, A., Firouz, R. M. & Illikainen, M. Drying shrinkage in alkali-activated binders–a critical review. *Constr. Build. Mater.* **190**, 533–550 (2018).
124. Yu, H., Meng, T., Zhao, Y., Liao, J. & Ying, K. Effects of basalt fiber powder on mechanical properties and microstructure of concrete. *Case Stud. Constr. Mater.* **17**, e01286 (2022).
125. Yao, X., Yang, T. & Zhang, Z. Compressive strength development and shrinkage of alkali-activated fly ash–slag blends associated with efflorescence. *Mater. Struct.* **49**, 2907–2918 (2016).
126. Ye, H., Cartwright, C., Rajabipour, F. & Radlińska, A. Understanding the drying shrinkage performance of alkali-activated slag mortars. *Cem. Concr. Compos.* **76**, 13–24 (2017).
127. Yip, C. K., Lukey, G. & Van Deventer, J. S. The coexistence of geopolymeric gel and calcium silicate hydrate at the early stage of alkaline activation. *Cem. Concr. Res.* **35** (9), 1688–1697 (2005).
128. Yuan, B., Yu, Q. & Brouwers, H. Assessing the chemical involvement of limestone powder in sodium carbonate activated slag. *Mater. Struct.* **50**, 1–14 (2017).
129. Zhang, X., Wang, W., Zhang, Y. & Gu, X. Research on hydration characteristics of OSR-GGBFS-FA alkali-activated materials. *Constr. Build. Mater.* **411**, 134321 (2024).
130. Qu, M. et al. A novel alkali-activated cement from mineral admixture, superabsorbent polymers, and alkali-doped carboxylate glass. *Constr. Build. Mater.* **383**, 131459 (2023).
131. Zheng, Y., Rao, F., Tian, X. & Lin, S. Synergistic gel formation in geopolymers of superior mechanical strength synthesized with volcanic Ash and slag. *Environ. Sci. Pollut. Res.* **30** (10), 26244–26255 (2023).
132. Rashad, A. M., Haraz, O. M., Elboushi, A. & Morsi, W. M. Electrical properties of alkali-activated materials against Portland cement. *Proc. Institution Civil Engineers-Construction Mater.* **176** (1), 33–44 (2023).
133. Benli, A. Sustainable use of waste glass sand and waste glass powder in alkali-activated slag foam concretes: Physico-mechanical, thermal insulation and durability characteristics. *Constr. Build. Mater.* **438**, 137128 (2024).
134. Burciaga-Díaz, O., Gómez-Zamorano, L. Y. & Escalante-García, J. I. Influence of the long term curing temperature on the hydration of alkaline binders of blast furnace slag-metakaolin. *Constr. Build. Mater.* **113**, 917–926 (2016).
135. Dai, X., Aydin, S., Yardimci, M. Y. & De Schutter, G. Fresh and hardened state properties, reaction kinetics and microstructure of sodium sulfate/sodium hydroxide–Activated slag mixtures. *Constr. Build. Mater.* **401**, 132943 (2023).
136. Moustapha, B. E. et al. Compensation of the negative effects of micro-encapsulated phase change materials by incorporating Metakaolin in geopolymers based on blast furnace slag. *Constr. Build. Mater.* **314**, 125556 (2022).
137. Gao, X., Yu, Q. & Brouwers, H. Assessing the porosity and shrinkage of alkali activated slag-fly Ash composites designed applying a packing model. *Constr. Build. Mater.* **119**, 175–184 (2016).
138. Li, Y. & Sun, Y. Preliminary study on combined-alkali–slag paste materials. *Cem. Concr. Res.* **30** (6), 963–966 (2000).
139. Ren, J. et al. A novel TiO2/Epoxy resin composited geopolymer with great durability in wetting-drying and phosphoric acid solution. *J. Clean. Prod.* **227**, 849–860 (2019).
140. Hoy, M., Rachan, R., Horpibulsuk, S., Arulrajah, A. & Mirzababaei, M. Effect of wetting–drying cycles on compressive strength and microstructure of recycled asphalt pavement–Fly Ash geopolymer. *Constr. Build. Mater.* **144**, 624–634 (2017).

Author contributions

Contribution statement Alaa M. Rashad: Conceptualization, Formal analysis, Project administration, Software, Supervision, Methodology, Validation, Visualization, Writing - original draft, Writing – review & editing. M. H. El-Nashar: Formal analysis, Software, Data curation, Methodology. Omnia Farouk Hussien: Software, Methodology. Reham Abu-Elwafa Mohamed: Investigation, Resources, Methodology, Supervision, Formal analysis, Data curation, Software.All authors read and approved the final manuscript.

Declarations

Competing interests

The authors declare no competing interests.

Additional information

Correspondence and requests for materials should be addressed to A.M.R.

Reprints and permissions information is available at www.nature.com/reprints.